Acta Pharmaceutica Sinica B 2025;15(8):3978−3996

Chinese Pharmaceutical Association
Institute of Materia Medica, Chinese Academy of Medical Sciences

Acta Pharmaceutica Sinica B

www.elsevier.com/locate/apsb
www.sciencedirect.com

PERSPECTIVE

FtsZ as a novel target for antibiotics development: Promises and challenges

Ming-Wei Wang[a,b,c,*], Kaini Hang[a,b], Wei Han[c], Xin Li[a], Qingtong Zhou[a,c], Dehua Yang[a,d]

[a]*Research Center for Deepsea Bioresources, Sanya 572025, China*
[b]*Department of Pharmacology, School of Basic Medical Sciences, Fudan University, Shanghai 200032, China*
[c]*Research Center for Medicinal Structural Biology, National Research Center for Translational Medicine at Shanghai, State Key Laboratory of Medical Genomics, Ruijin Hospital, Shanghai Jiao Tong University School of Medicine, Shanghai 200025, China*
[d]*State Key Laboratory of Chemical Biology and The National Center for Drug Screening, Shanghai Institute of Materia Medica, Chinese Academy of Sciences, Shanghai 201203, China*

Received 21 April 2025; received in revised form 12 May 2025; accepted 23 May 2025

KEY WORDS

FtsZ;
Cell division;
Drug target;
Cryo-electron microscopy;
Deepsea bacterium;
Antibiotics

Abstract Filamenting temperature-sensitive mutant Z (FtsZ), a protein essential for bacterial cell division, is highly conserved across bacterial species but absent in humans, positioning it as a strategic target for the development of antibiotics. Significant efforts to identify FtsZ inhibitors—*via* biochemical assays (*e.g.*, GTPase activity) and cellular approaches (*e.g.*, immunofluorescence)—have yielded over 100 natural products and synthetic compounds, whose cheminformatics clustering underscores a limited chemical diversity among the current scaffolds. Structural studies, including X-ray crystallography and cryo-electron microscopy, have resolved 97 FtsZ structures revealing conserved polymerization mechanisms and conformational plasticity, as exemplified by extremophile adaptations (*e.g.*, *Shewanella benthica* from the high-pressure environment of the Mariana Trench's Challenger Deep). However, clinical translation is hindered by weak binding affinities, inhibitory inefficacy, dynamic conformational flexibility, and evolving drug resistance linked to FtsZ's functional plasticity. To address these challenges, future efforts should be directed to resolve transient assembly intermediates, leveraging machine learning with high-throughput screening, and integrating structural biology with pharmacokinetic optimization. Multidisciplinary strategies combining these approaches hold promise for translating FtsZ-focused research into clinically viable therapies, addressing the critical unmet need posed by antibiotics resistance.

*Corresponding author.
E-mail address: mwwang@simm.ac.cn (Ming-Wei Wang).

Peer review under the responsibility of Chinese Pharmaceutical Association and Institute of Materia Medica, Chinese Academy of Medical Sciences.

https://doi.org/10.1016/j.apsb.2025.06.008

1. Introduction

Filamenting temperature-sensitive mutant Z (FtsZ), a key protein that initiates bacterial cell division, is crucial for the proliferation of diverse bacterial species[1]. FtsZ forms protofilaments that coalesce into the Z-ring at the division site through GTP-dependent polymerization (Fig. 1[2-6]). Although FtsZ shares structural similarities with tubulin, it exhibits a low sequence similarity (10%−18%) and is unaffected by classical antineoplastic agents such as nocodazole and paclitaxel, which do not inhibit its assembly or GTPase activity[1]. These unique features, combined with the high sequence conservation of FtsZ among bacteria, make it a promising therapeutic target for bacterial infections. Recent studies have demonstrated that FtsZ inhibitors can act synergistically with β-lactam antibiotics, suggesting a new strategy to combat multidrug-resistant pathogens such as methicillin-resistant *Staphylococcus aureus* (MRSA)[2].

FtsZ consists of four functional domains: an N-terminal segment, a core region comprising the nucleotide-binding domain (NBD) and the C-terminal GTPase-activating domain

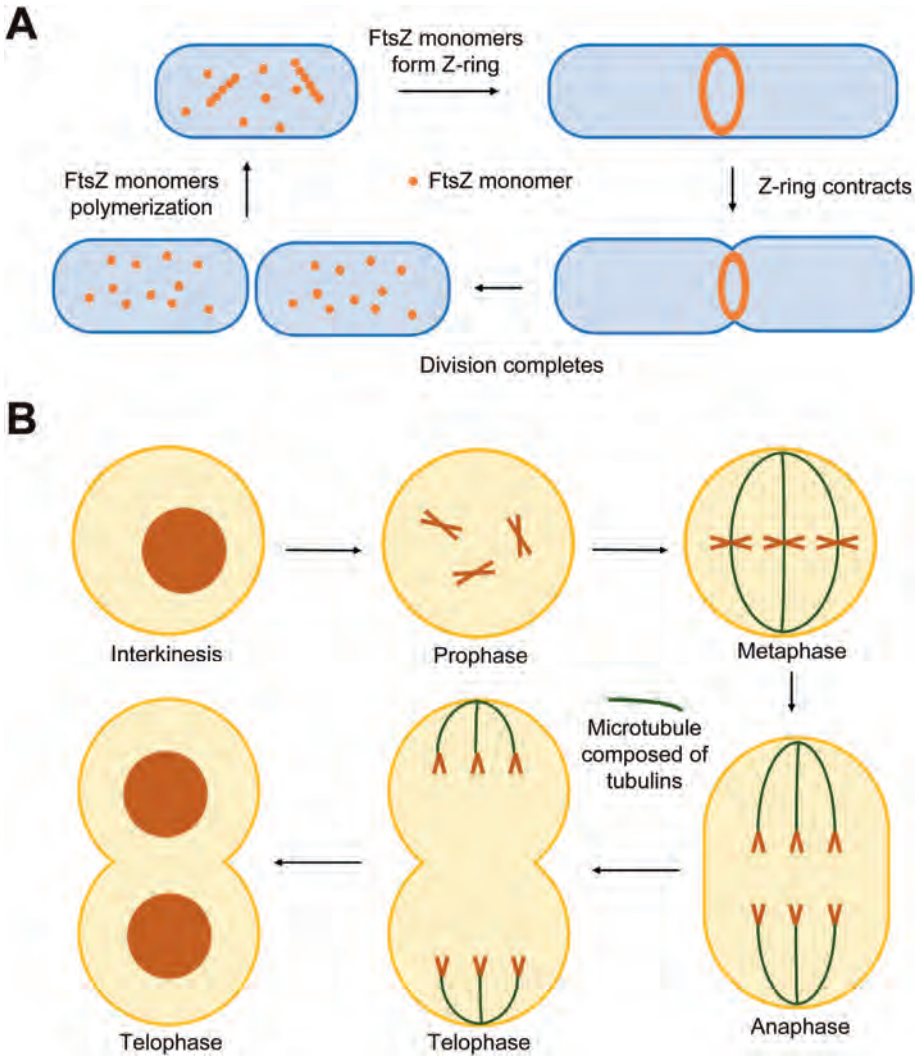

Figure 1 Schematic diagram illustrating the roles of FtsZ in bacterial division and tubulin in mitosis. (A) Bacterial division and proliferation mediated by filamenting temperature-sensitive mutant Z (FtsZ)[2,3]. FtsZ, a tubulin-like GTPase, polymerizes into protofilaments in the presence of GTP, forming a Z-ring at the midcell. The Z-ring attaches to the cell membrane and recruits division proteins, including FtsA[4] and ZipA[5], to assemble the divisome complex. The Z-ring then contracts, driven by GTP hydrolysis, facilitating the formation of a septum and ultimately dividing the cell into two daughter cells. (B) Role of tubulin in human cell mitosis[6]. During metaphase and anaphase, tubulin α- and β-subunits form heterodimers that assemble into microtubules. These spindle microtubules align and segregate chromosomes, ensuring the precise distribution of sister chromatids to opposite poles of the cell, thus guaranteeing equal chromosome inheritance in the two daughter cells.

(GAD) separated by the H7 helix, a variable spacer, and a C-terminal peptide involved in interactions with regulatory components[7-10] (Fig. 2[4,5,9-11]). They collectively enable FtsZ to polymerize into protofilaments and form the Z-ring, a key structure for bacterial cytokinesis. A variety of FtsZ inhibitors, including peptides, natural products, and synthetic small molecules, have been developed to target specific regions of the protein. These inhibitors interact with the nucleotide-binding pocket in the N terminus, the cleft between the central helix H7 and the C terminus, or the C-terminal domain itself, thereby preventing GTP binding, FtsZ monomer polymerization, or the binding of regulatory components such as zinc-finger protein A (ZipA)[12]. However, none of them have advanced to phase 2 clinical trials, largely due to an incomplete understanding of their mechanisms of action.

To systematically evaluate progress in FtsZ-focused research, we reviewed the studies published from 2003 to 2024 and queried the databases, including the Protein Data Bank (PDB) and BindingDB, for reported FtsZ structures and inhibitors, respectively. As of April 2025, 97 FtsZ structures from 12 bacterial species (16 strains) have been reported, including common pathogens such as *Staphylococcus aureus* (Supporting Information Table S1). These structures have provided critical insights into the conformational dynamics and polymerization mechanisms of FtsZ and its interactions with inhibitors. In this perspective, we expand the structural landscape further by determining the cryo-electron microscopy (cryo-EM) density map of FtsZ from the deepsea bacterium *Shewanella benthica* (SbFtsZ), which thrives under the high-pressure, low-temperature, and high-salinity conditions of the Mariana Trench's Challenger Deep. Biochemical and cellular studies have identified over 100 inhibitors targeting FtsZ's nucleotide-binding pocket, binding cleft, and allosteric sites. However, clinical translation remains hindered by weak binding affinities, conformational flexibility, and evolving resistance linked to FtsZ's functional plasticity. This perspective synthesizes structural, biochemical, and cheminformatics data to outline the opportunities, challenges, and strategies for advancing FtsZ-targeted antimicrobial drug development.

2. Role in cell division

Cytokinesis, essential to cell division, is a fundamental phenomenon across all life forms[13]. In bacteria, this crucial task is orchestrated by the divisome, a multiple protein complex that facilitates and regulates the process[13,14]. FtsZ is the key protein that initiates cell division, facilitating proliferation across diverse bacterial species[6,15]. As a tubulin homolog GTPase, FtsZ forms protofilaments that subsequently coalesce into the Z-ring at the designated site of division *via* its GTP-dependent polymerization[16,17], a step indispensable for the bacterial cytokinesis[6,18,19]. The assembly of FtsZ is regulated by nucleotide binding and protein−protein interaction, alongside post-translational modifications and environmental factors such as temperature, pH, and osmolarity, ensuring precise division control[2]. The treadmilling of

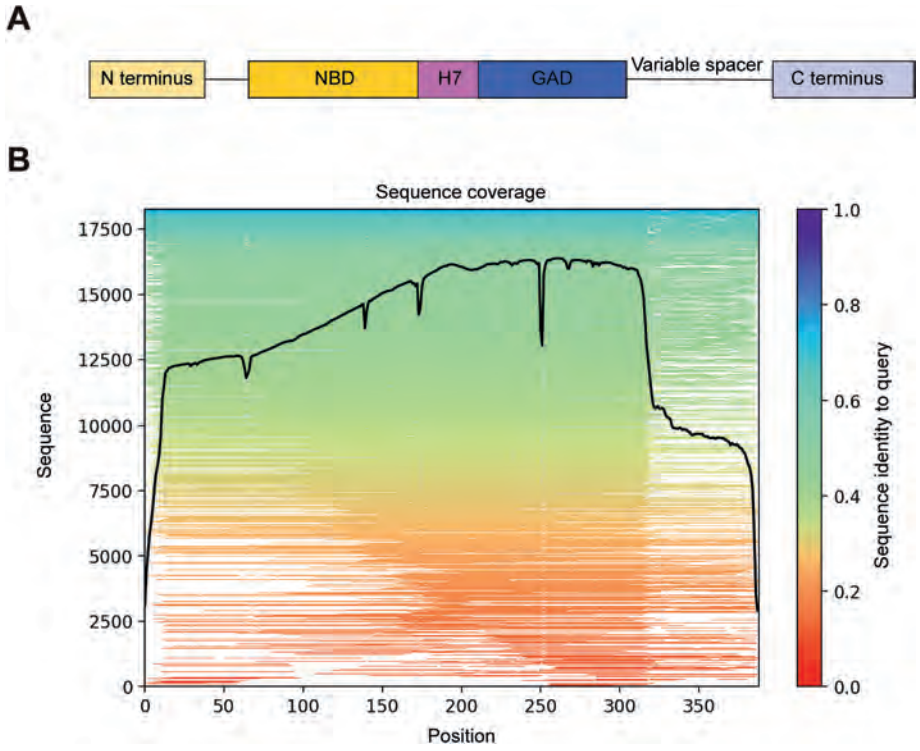

Figure 2 The domain structure of FtsZ and its sequence coverage across diverse species. (A) The core region, consisting of the nucleotide-binding domain (NBD) and the C-terminal GTPase-activating domain (GAD), is separated by the H7 helix[9,10]. This region displays the highest similarity to human tubulin and is essential to GTP binding, hydrolysis, and protofilament assembly. The N terminus is highly variable, with its precise functions currently unknown. The variable spacer and C terminus, which interact with other cell division proteins recruited by FtsZ, such as ZipA[5] and FtsA[4], play a critical role in anchoring the Z-ring to the membrane, but exhibit less sequence conservation across species. (B) Comparison of multiple sequence alignment (MSA) length and per-position sequence coverage for FtsZ across 18,000 species, as predicted by AlphaFold 3[11].

FtsZ, a process where the protofilament undergoes polymerization at one end (plus-end) and depolymerization at the other end (minus-end), drives cell wall synthesis, resulting in the contraction of the Z-ring and the formation of the septum of cells[3] (Fig. 1A). Positioned at the midpoint of the cell, the Z-ring recruits over 30 partner proteins, such as filamentous temperature-sensitive protein A (FtsA)[4], ZipA[5], EzrA[20], caseinolytic mitochondrial matrix peptidase chaperone subunit X (ClpX)[21], septum-forming protein (SepF)[22] and minicell division protein C (MinC)[23], coordinating the assembly and contraction of the Z-ring to ensure precise cell division[22].

The mitosis of human cells is fundamentally different from bacterial division involving a highly regulated spindle apparatus composed of tubulin. It consists of four phases: prophase, metaphase, anaphase, and telophase. During prophase, the spindle apparatus begins to form and connects with the chromosomes in metaphase. In anaphase, the spindle fibers pull the sister chromatids apart and move them toward the opposite poles of the cell. The spindle apparatus ensures that the two daughter cells receive an equal number of chromosomes after division (Fig. 1B). Microtubules, the primary component of the spindle apparatus, are composed of tubulin with two subunits (α and β) in the form of heterodimers. Although FtsZ and tubulin are homologous, their roles in cell division are entirely different.

3. Screening for FtsZ inhibitors

Several screening assays have been developed to identify FtsZ inhibitors, including GTPase, polymerization, immunofluorescence, and cellular activity[12,24,25]. While GTPase and polymerization assays are adapted to a high-throughput format, immunofluorescence and cell-based approaches offer more physiological relevance.

3.1. GTPase assay

GTP hydrolysis by FtsZ is coupled to NADH oxidation, which can be monitored by fluorescence intensity. In the absence of an inhibitor, FtsZ hydrolyzes GTP to GDP. The hydrolyzed GDP is then converted back to GTP in the presence of phosphoenolpyruvate and pyruvate kinase, transforming NADH to NAD^+. Fluorescence of NADH can thus be measured to indirectly assess FtsZ activity[25]. This assay provides real-time, high-throughput measurement of FtsZ hydrolysis *via* fluorescence, but requires careful background subtraction, high-purity reagents and can obscure the distinction between effects on polymerization versus catalysis.

3.2. Polymerization assay

It measures FtsZ filament assembly through light scattering, where the intensity of light scattering is proportional to the amount of FtsZ polymer formed[26]. In this assay, FtsZ polymerization is induced by [γ-^{32}P]GTP, and the extent of polymerization is inferred from changes in light scattering. In the presence of an inhibitor, FtsZ polymerization is hindered, resulting in decreased light scattering[27]. This assay provides label-free, convenient, and real-time monitoring of filament assembly, but cannot resolve filament morphology or distinguish small oligomers from large bundles, often necessitating confirmatory EM or sedimentation analysis.

3.3. Immunofluorescence assay

It observes Z-ring morphology during cell division. Candidate inhibitors are added to the culture medium of logarithmic-phase *Escherichia coli*, and immunoreaction is performed using polyclonal antibodies against FtsZ and fluorescein isothiocyanate (FITC)-conjugated secondary antibodies. Changes in Z-ring and cell structure are then examined under an electron microscope[25], thereby assessing the inhibitory effects of potential FtsZ inhibitors. Yet its low throughput, dependence on high-quality antibodies, labor-intensive sample preparation and end-point/semi-quantitative nature make it best suited to secondary validation rather than primary screening.

3.4. Cell-based assay

It detects inhibitors by monitoring the sporulation process of bacteria. In the absence of an inhibitor, the expression of the *spoIIA-lacZ* gene is activated during sporulation, leading to the production of β-galactosidase and transcription factors in the cytoplasm. This process is disrupted by FtsZ inhibitors, preventing the activation of *spoIIQ* and the synthesis of β-glucuronidase[28]. While powerful for identifying compounds that block septation, they generate broad hit lists requiring rigorous secondary assays to confirm direct FtsZ engagement and to eliminate general cytotoxins.

4. Reported FtsZ inhibitors

A number of inhibitors derived from natural products or synthetic compounds have been reported (Table 1[29-62]), demonstrating various bioactivities against FtsZ.

4.1. Natural product derivatives

Berberine, a natural alkaloid derived from *Berberis* plants and traditionally used in Chinese medicine, inhibits FtsZ GTPase activity and dynamic polymerization[8,22,41]. Domadia et al.[63] demonstrated in 2008 that berberine interacts with key structural motifs of FtsZ, including dimethoxy groups, the isoquinoline nucleus, and the benzodioxolo ring, as revealed by saturation transfer difference nuclear magnetic resonance (NMR) spectroscopy. Subsequent studies by Sun et al.[64] introduced alkoxy benzene substituents to create derivatives with potent activity against Gram-positive bacteria, such as MRSA and vancomycin-resistant enterococcus (VRE), with minimum inhibitory concentration (MIC) values ranging from 2 to 16 μg/mL.

Cinnamaldehyde, a natural aromatic compound extracted from cinnamon bark, inhibits FtsZ GTPase activity (IC_{50}: 5.81 μmol/L) and dynamic polymerization (IC_{50}: 6.86 μmol/L) by binding to the C-terminal T7 loop of FtsZ[27]. Derivatives of cinnamaldehyde demonstrated inhibitory effects on *Staphylococcus aureus* (ATCC25923) division at concentrations ranging from 0.25 to 4 μg/mL[39,56].

Chrysophaentins A−H, isolated from marine algae, exhibit strong antibacterial activity against MRSA and *Streptococcus pneumoniae*, with MIC values of 1.5 μg/mL and 2.9 μg/mL, respectively. These compounds competitively bind to the GTP-binding site of FtsZ, as confirmed by NMR, and inhibit the FtsZ GTPase activity of *Escherichia coli* (IC_{50}: 6.7 μg/mL)[45]. Modified derivatives, such as compound 6, have shown inhibitory effects on

Table 1 Reported FtsZ inhibitors.

Organism	Chemical name/ PubChem ID	Biological activity	Organism	Chemical name/ PubChem ID	Biological activity
Aquifex aeolicus	BrGTP (CID: 136188778)	37 μmol/L (IC_{50})/ 126 nmol/L (K_d)[29]	*Klebsiella pneumoniae*	Levofloxacin (CID: 149096)	2−4 μg/mL (MIC)[30]
	C8-morpholino-GTP (CID: 135566333)	714 nmol/L (K_d)[29]	*Mycobacterium smegmatis*	CID: 71589851	3.3 μg/mL (MIC)[31]
	ClGTP (CID: 136188774)	35 μmol/L (IC_{50})/ 77 nmol/L (K_d)[29]	*Mycobacterium tuberculosis*	4-hydroxycoumarin (CID: 54682930)	NA[32]
	IGTP (CID: 136188780)	44 μmol/L (IC_{50})/ 71 nmol/L (K_d)[29]		Atovaquone (CID: 19373432)	10 μg/mL (MIC)[33]
	MeGTP (CID: 136188776)	44 μmol/L (IC_{50})[29]		CID: 418898	34.2 μmol/L (IC_{50})[34]
	MeOGTP (CID: 136188770)	10 μmol/L (IC_{50})/ 3.33 nmol/L (K_d)[29]		CID: 3010938	38.1 μmol/L (IC_{50})[34]
	PhGTP (CID: 136188784)	71 μmol/L (IC_{50})[29]		CID: 6480506	52 μmol/L (IC_{50})[34]
	PyrrGTP (CID: 136188772)	15 μmol/L (IC_{50})/ 15.6 nmol/L (K_d)[29]		CID: 25100998	6.21 μmol/L (IC_{50})[35]
	tBuGTP (CID: 136188782)	41 μmol/L (IC_{50})/ 91 nmol/L (K_d)[29]		CID: 25101148	7.69 μmol/L (IC_{50})[35]
Bacillus subtilis	BDBM50439496 (CID: 60164930)	70 μmol/L (IC_{50})[36]		CID: 57390524	27.3 μmol/L (IC_{50})[34]
	BDBM50581024 (CID: 59402956)	1.3 μmol/L (K_d)[37]		CID: 57390525	18.6 μmol/L (IC_{50})[34]
	BDBM50581026 (CID: 156022394)	700 nmol/L (K_d)[37]		CID: 57392294	34.1 μmol/L (IC_{50})[34]
	CID: 2889	30 μmol/L (IC_{50})[38]		CID: 57392416	26.8 μmol/L (IC_{50})[34]
	CID: 1275778	1.5 μmol/L (K_d)[39]		CID: 57394045	46.2 μmol/L (IC_{50})[34]
	CID: 27186897	9.3 μmol/L (K_d)[37]		CID: 57395806	34.8 μmol/L (IC_{50})[34]
	CID: 71589851	6.7 μg/mL (MIC)[31]		CID: 57399372	34.3 μmol/L (IC_{50})[34]
	CID: 166627255	1.9 μmol/L (K_d)[37]		CID: 57401033	16.4 μmol/L (IC_{50})[34]
	CID: 166627260	1.1 μmol/L (K_d)[37]		CID: 57402789	21 μmol/L (IC_{50})[34]
	CID: 166627334	15 μmol/L (K_d)[37]		CID: 57402790	54.6 μmol/L (IC_{50})[34]
	CID: 166627877	6.7 μmol/L (K_d)[37]		CID: 57402791	29.5 μmol/L (IC_{50})[34]
	CID: 166630204	9.5 μmol/L (K_d)[37]		CID: 57402792	46 μmol/L (IC_{50})[34]
	CID: 166630397	71 μmol/L (K_d)[37]		CID: 57402899	45.7 μmol/L (IC_{50})[34]
	CID: 166631443	5.9 μmol/L (K_d)[37]		Isoniazid (CID: 3767)	0.25−4 μg/mL (MIC)[30]
	CID: 166632438	7.1 μmol/L (K_d)[37]		Nebivolol (CID: 71301)	25 μg/mL (MIC)[33]
	CID: 166634198	200 nmol/L (K_d)[37]		Paroxetine (CID: 43815)	25 μg/mL (MIC)[33]
	CID: 166634961	1.9 μmol/L (K_d)[37]		Rifampin (CID: 135398735)	0.25−4 μg/mL (MIC)[30,33]
	CID: 166635393	3.8 μmol/L (K_d)[37]		Sitagliptin (CID: 4369359)	150 μg/mL (MIC)[33]
	CID: 166636292	1.5 μmol/L (K_d)[37]		Streptomycin (CID: 19649)	0.5 μg/mL (MIC)[33]
	CID: 166636439	8.0 μmol/L (K_d)[37]		Tribromophenol (CID: 1483)	2−4 μg/mL (MIC)[30]
	Cinnamaldehyde (CID: 637511)	500 μg/mL (MIC)[27]		Totarol (CID: 92783)	11 μmol/L (K_d)[39]

Table 1 (*continued*)

Organism	Chemical name/ PubChem ID	Biological activity	Organism	Chemical name/ PubChem ID	Biological activity
	DFMBA (CID: 3544383)	670 μmol/L (K_d)[37]	*Staphylococcus aureus*	BDBM50439496 (CID: 60164930)	38 μmol/L (IC_{50})[36,39]
	Gossypol (CID: 3503)	4 μg/mL (MIC)[40]		Berberine (CID: 2353)	10 μmol/L (IC_{50})[41]
	Honokiol (CID: 72303)	4 μg/mL (MIC)[42]		BOFP (CID: 145945984)	3.14 μmol/L (K_d)[43]
	Morusin (CID: 5281671)	1−4 μg/mL (MIC)[44]		Chrysophaentin A (CID: 46872004)	67 μmol/L (IC_{50})[36]/ 1.5 μg/mL (MIC)[45]
	PC190723 (CID: 25016417)	100 nmol/L (K_d)[37]/1 μg/mL (MIC)[46]		CID: 3100357	32 μg/mL (MIC)[24]
	Plumbagin (CID: 10205)	15.8 μmol/L (K_d)[47]		CID: 3123338	8 μg/mL (MIC)[24]
	Purpurin (CID: 6683)	5.2 μmol/L (K_d)[47]		CID: 45360432	37.5 μmol/L (IC_{50})[8,41]
	Sanguinarium (CID: 5154)	3 μmol/L (IC_{50})[48]		CID: 45360437	55.7 μmol/L (IC_{50})[41]
	Totarol (CID: 92783)	24 μmol/L (IC_{50})[49]/2 μg/mL (MIC)[50]		CID: 45360475	77.2 μmol/L (IC_{50})[41]
Enterococcus faecalis	BOFP (CID: 145945984)	4.62 μmol/L (K_d)[43]		CID: 46907295	37.8−77.4 μmol/L (IC_{50})[8,41]
	Honokiol (CID: 72303)	12 μg/mL (MIC)[42]		CID: 49842394	2 μmol/L (K_d)[51]
	Viriditoxin (CID: 53343291)	2−16 μg/mL (MIC)[52]		CID: 68470071	600 nmol/L (K_d)[53]
Escherichia coli	BDBM50439496 (CID: 60164930)	37 μmol/L (IC_{50})[39]		CID: 71462731	3.5 μmol/L (K_d)[54]
	Berberine (CID: 2353)	10 μmol/L (IC_{50})[8]/23 nmol/L (K_d)[22]		CID: 71463184	5.4 μmol/L (K_d)[51]
	BOFP (CID: 145945984)	0.44 μmol/L (K_d)[43]		CID: 168278889	3.86 μmol/L (K_d)[55]
	Chrysophaentin A (CID: 46872004)	9.87 μmol/L (IC_{50})[39]		CID: 168278977	2.38 μmol/L (K_d)[55]
	CID: 2954	16.6 μmol/L (K_d)[39]		CID: 168291798	2.49 μmol/L (K_d)[55]
	CID: 3032920	10.5 μmol/L (IC_{50})[39]		Cinnamaldehyde (CID: 637511)	250 μg/mL (MIC)[27]
	CID: 16662249	8.3 μmol/L (IC_{50})[39]		FtsZ−IN−1 (CID: 163322356)	3.84 μmol/L (K_d)[55]
	CID: 71462731	3.8 μmol/L (K_d)[54]		Gossypol (CID: 3503)	8 μg/mL (MIC)[40]
	CID: 71589851	10 μg/mL (MIC)[31]		Honokiol (CID: 72303)	4−8 μg/mL (MIC)[42]
	CID: 84377541	90.5 μmol/L (IC_{50})[56]		Levofloxacin (CID: 149096)	0.25 μg/mL (MIC)[30]
	CID: 118734492	12 μmol/L (IC_{50})[39]		Linezolid (CID: 441401)	2 μg/mL (MIC)[57]
	CID: 118736485	24 μmol/L (IC_{50})[58]		PC190723 (CID: 25016417)	150−154 nmol/L (IC_{50})[8,39,55]/ 1 μg/mL (MIC)[46]
	CID: 118736488	30 μmol/L (IC_{50})[58]		Silibinin (CID: 31553)	75 μmol/L (IC_{50})[59]
	CID: 118736489	95 μmol/L (IC_{50})[58]		TXA707 (CID: 90135655)	1 μg/mL (MIC)[57,60]
	CID: 118736490	28 μmol/L (IC_{50})[58]		TXA6101 (CID: 72947301)	0.125 μg/mL (MIC)[60]
	CID: 118736491	30 μmol/L (IC_{50})[58]		TXH9179 (CID: 167312464)	0.25 μg/mL (MIC)[57]

(*continued on next page*)

Table 1 (*continued*)

Organism	Chemical name/ PubChem ID	Biological activity	Organism	Chemical name/ PubChem ID	Biological activity
	CID: 118736492	58 μmol/L (IC_{50})[58]		Vancomycin (CID: 14969)	1 μg/mL (MIC)[57]
	CID: 118736494	49 μmol/L (IC_{50})[58]		Viriditoxin (CID: 53343291)	4−8 μg/mL (MIC)[52]
	CID: 118736568	26 μmol/L (IC_{50})[58]		ZI1 (CID: 90123239)	0.06 μg/mL (MIC)[61]
	CID: 118736571	65 μmol/L (IC_{50})[58]	*Staphylococcus epidermidis*	Honokiol (CID: 72303)	4 μg/mL (MIC)[42]
	CID: 118736576	52 μmol/L (IC_{50})[58]		PC190723 (CID: 25016417)	1 μg/mL (MIC)[46]
	CID: 118736580	85 μmol/L (IC_{50})[58]	*Staphylococcus haemolyticus*	PC190723 (CID: 25016417)	0.5 μg/mL (MIC)[46]
	CID: 118736581	24 μmol/L (IC_{50})[58]	*Staphylococcus hominis*	PC190723 (CID: 25016417)	1 μg/mL (MIC)[46]
	CID: 118736582	14 μmol/L (IC_{50})[58]	*Staphylococcus lugdunensis*	PC190723 (CID: 25016417)	1 μg/mL (MIC)[46]
	CID: 118988516	27 μmol/L (IC_{50})[58]	*Staphylococcus saprophyticus*	PC190723 (CID: 25016417)	1 μg/mL (MIC)[46]
	CID: 118988515	9 μmol/L (IC_{50})[58]	*Staphylococcus warneri*	PC190723 (CID: 25016417)	1 μg/mL (MIC)[46]
	Cinnamaldehyde (CID: 637511)	5.81 μmol/L (IC_{50})[39]	*Streptococcus pneumoniae*	BOFP (CID: 145945984)	0.82 μmol/L (K_d)[43]
	Dichamanetin (CID: 181193)	12.5 μmol/L (IC_50)[39]		Chrysophaentin A (CID: 46872004)	2.9 μg/mL (MIC)[45]
	Gossypol (CID: 3503)	128 μg/mL (MIC)[40]	*Pseudomonas aeruginosa*	BOFP (CID: 145945984)	0.58 μmol/L (K_d)[43]
	Levofloxacin (CID: 149096)	0.03−4 μg/mL (MIC)[30]		Levofloxacin (CID: 149096)	4 μg/mL (MIC)[30]
	Purpurin (CID: 6683)	11 μmol/L (K_d)[47]	*Xanthomonas oryzae*	Chelerythrine chloride (CID: 72311)	0.93 μg/mL (MIC)[62]
	Sanguinarium (CID: 5154)	3−13.8 μmol/L (IC_{50})[41,48]		Sanguinarine chloride (CID: 68635)	0.96 μg/mL (MIC)[62]

CID, PubChem Compound Identification; IC_{50}, half maximal inhibitory concentration; K_d, dissociation constant; MIC, minimum inhibitory concentrations; NA, data not available.

the FtsZ GTPase activity of *Staphylococcus aureus* and *Escherichia coli* with IC_{50} values of approximately 37 μmol/L[36].

Viriditoxin, derived from *Aspergillus viridinutans*, effectively inhibits the GTPase activity (IC_{50}: 7.0 μg/mL) and polymerization (IC_{50}: 8.2 μg/mL) of FtsZ, disrupting Z-ring formation and bacterial cell division. It displays potent activity against drug-resistant Gram-positive pathogens, including MRSA and *Enterococcus faecium*, with MIC values of 2−16 μg/mL[52].

Curcumin, a natural polyphenol from turmeric (*Curcuma longa*), destabilizes FtsZ protofilaments by enhancing GTP hydrolysis, thereby disrupting Z-ring assembly and suppressing the growth of *Bacillus subtilis* and *Escherichia coli*[38,65].

Purpurin, an anthraquinone from madder plants, interferes with Z-ring localization by binding to the nucleotide-binding site of FtsZ, reducing GTP hydrolysis without affecting microtubule polymerization[47]. Similarly, totarol, a diterpene phenol isolated from *Siraitia grosvenorii*, reduces the assembly of FtsZ protofilaments and inhibits GTPase activity, demonstrating potent activity against Gram-positive bacteria, including *Mycobacterium tuberculosis*, *Bacillus subtilis*, and *Staphylococcus aureus*[50,66].

4.2. Synthetic compounds

3-Methoxybenzamide (3-MBA) targets FtsZ and inhibits cell division in *Bacillus subtilis*[67]. PC190723, a representative benzamide derivative discovered by Czaplewski's group[46], exhibits strong antibacterial activity against Gram-positive bacteria, including *Bacillus subtilis* and MRSA, with an MIC as low as 1 μg/mL. Treatment with PC190723 causes *Bacillus subtilis* cells to elongate and *Staphylococcus aureus* cells to increase in volume, indicating inhibited cell division[67]. Molecular docking suggests that PC190723 binds between the C-terminus and the H7 helix of FtsZ[46]. However, its pharmacokinetics profiles in animal studies were unsatisfactory. Kaul et al.[68] developed analogs with improved metabolic stability and antibacterial efficacy, including TXA436, TXA707, and TXA709, with TXA709 completed phase 1 clinical trials for MRSA infections.

Quinolines[69], originally used to treat malaria, have been modified to target FtsZ. LaVoie et al. designed 3-phenylisoquinoline derivatives, with compound 6b showing MIC values of 1 μg/mL against MRSA and 4 μg/mL against

Enterococcus faecalis[51]. Sun et al.[70] found that *N*-methylbenzindolo[3,2-*b*]quinoline and *N*-methylbenzofurano[3,2-*b*]quinoline derivatives, had strong antibacterial activity against MRSA and VRE by inhibiting FtsZ GTPase activity, disrupting Z-ring formation, and blocking bacterial division[70,71].

Ruiz-Avila et al.[72] used molecular docking to screen small-molecule FtsZ inhibitors that compete with GTP and discovered that UCM05, UCM44, and UCM53 significantly inhibited bacterial growth, with MIC values of 100, 25, and 13 μmol/L, respectively. These compounds induced cell elongation in *Bacillus subtilis* and disrupted Z-ring formation. Structural optimization led to biphenyl derivative **28** showing a strong binding affinity to FtsZ (K_d: 0.5 μmol/L) and better antibacterial activity against MRSA (MIC: 7 μmol/L)[73].

5. Chemical similarity of FtsZ inhibitors

To systematically analyze the chemical similarity among reported FtsZ inhibitors, we performed comprehensive queries of the BindingDB database (https://www.bindingdb.org/) and conducted an extensive literature search spanning from 2003 to 2024. A total of 215 experimental activity data points were collected and then filtered to remove redundancy (*e.g.*, multiple entries for the same molecule studied against different bacterial strains), resulting in 114 unique FtsZ inhibitors, including some well-known compounds. Pairwise Tanimoto coefficients[74] were calculated, and a complex network was generated where nodes represent inhibitors (light green) and edge thickness indicates chemical similarity (Fig. 3A[74,75]). Clustering identified three major classes (classes I−III) and isolated nodes with weak similarity to others, such as berberine, vancocin, nebivolol, rifampicin, chrysophaentins, sanguinarium, paroxetine, and cinnamaldehyde.

Class I comprises 51 members, including 19 compounds with common names. The most representative molecule with highest clustering coefficient is BDBM50581031 (PubChem CID: 166634961). PC190723, TXA707, and TXH9179 exemplify the structural and functional diversity within this class (Fig. 3B). PC190723, a 2,6-difluoro-3-methoxybenzamide derivative[46,76,77],

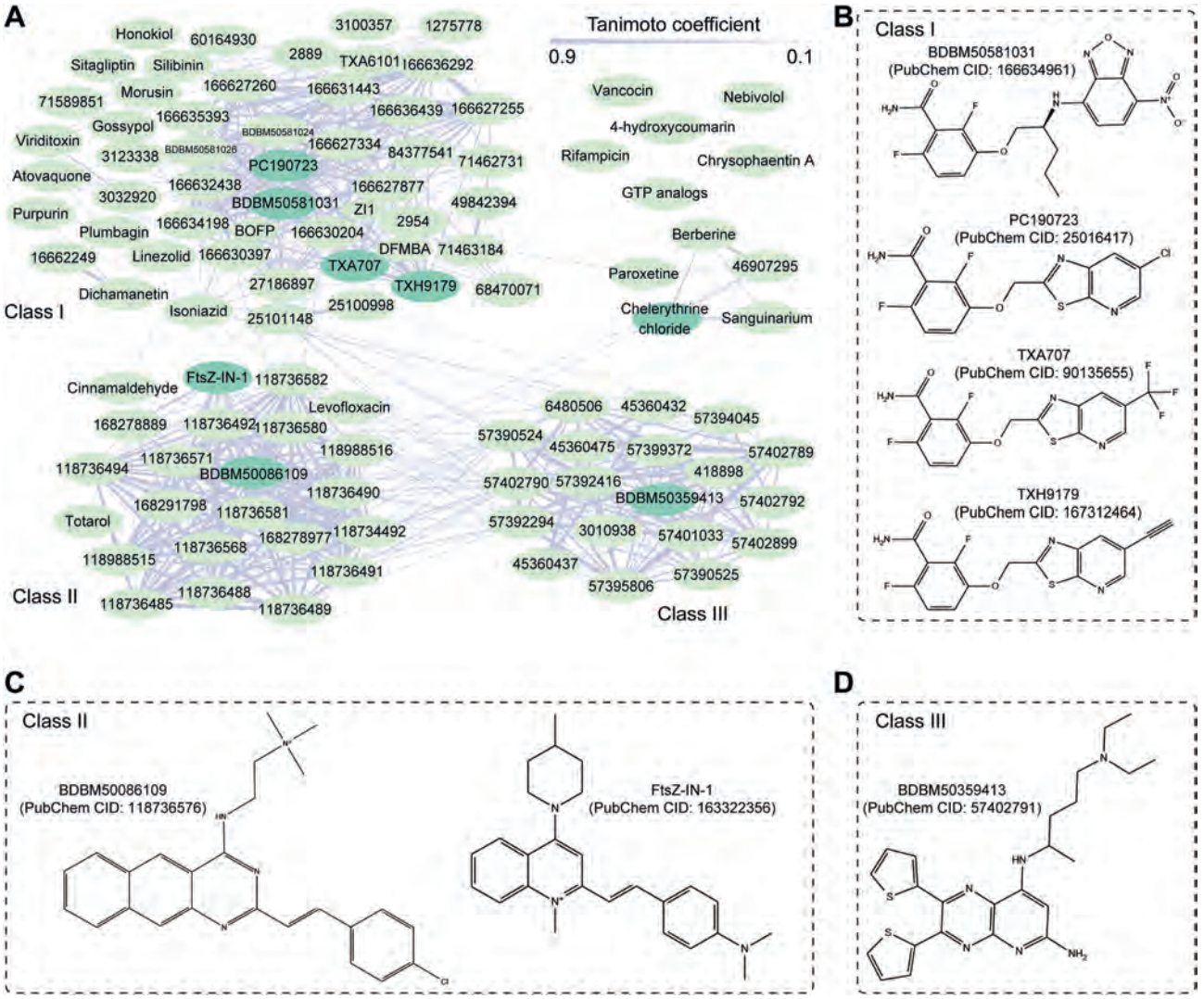

Figure 3 Chemical similarity analysis of 114 FtsZ inhibitors reported in the literature from 2003 to 2024. (A) Structural similarity network of FtsZ inhibitors visualized by Cytoscape v.3.10.2[75]. Each node represents an FtsZ inhibitor (light green), with edge thickness indicating the degree of chemical similarity using the Tanimoto coefficient[74]. The inhibitors are divided into three classes, with representative inhibitors highlighted in cyan. (B−D) Chemical structures of representative inhibitors from class I (B), class II (C), and class III (D).

shows limited efficacy against Gram-negative bacteria, likely due to outer membrane permeability barriers and efflux mechanisms. TXA707 disrupts FtsZ polymerization dynamics, preventing Z-ring formation and bacterial cell division[78,79]. It exhibits strong activity against MRSA and enhances β-lactam efficacy, thereby increasing antibiotic susceptibility. TXH9179, an optimized TXA707 derivative with a 6-ethynyl substituent, adopts a linear binding mode, improving inhibitory potency and reducing resistance frequency[57]. It displays a broad-spectrum activity against multidrug-resistant Gram-positive pathogens, including linezolid-resistant *Staphylococcus* (LRSA), vancomycin-intermediate *Staphylococcus aureus* (VISA) and vancomycin-resistant *Staphylococcus* (VRSA), and favorable pharmacokinetics for oral and intravenous administration[57]. These three inhibitors share a benzamide core while exhibiting distinct structural modifications.

Class II consists of 23 members, including 4 compounds with common names (Fig. 3C). The structurally central molecule is BDBM50086109 (PubChem CID: 118736576), with an IC_{50} of 52 μmol/L in enzyme-coupled GTPase assay[58]. FtsZ-IN-1, a quinolinium ring-containing inhibitor, exhibits strong antibacterial activity against Gram-positive bacteria, with MICs ranging from 0.5 to 8 μg/mL[55]. Unlike polymerization-disrupting inhibitors, FtsZ-IN-1 enhances FtsZ assembly, leading to aberrant polymerization and subsequent cell elongation in *Bacillus subtilis*. This mechanism effectively disrupts bacterial cytokinesis, making FtsZ-IN-1 a unique modulator of FtsZ dynamics.

Class III has 19 members, none of which has a common name, suggesting that the molecules in this cluster have been less extensively studied. The most structurally central compound is BDBM50359413 (PubChem CID: 57402791)[34] (Fig. 3D). It inhibited FtsZ polymerization of *Mycobacterium tuberculosis* (expressed in *Escherichia coli*), as confirmed *via* light scattering assay with an IC_{50} value of 29.5 μmol/L, but it showed a CC_{50} (cytotoxic concentration 50%) value in Vero cells of 5.9 μmol/L[34].

6. Molecular architecture of FtsZ

Most FtsZ structures are crystal structures, displaying significant molecular plasticity within FtsZ. The first structure, determined in *Methanocaldococcus jannaschii* (MjFtsZ, PDB code: 1FSZ) in 1998, provided the foundational understanding of this protein[80,81]. Since then, high-resolution structures from various bacteria, such as *Pseudomonas aeruginosa* (PaFtsZ, PDB code: 2VAW)[82], *Mycobacterium tuberculosis* (MtbFtsZ, PDB code: 2Q1Y)[83], *Bacillus subtilis* (BsFtsZ, PDB code: 2RHL)[84], *Staphylococcus aureus* (SaFtsZ, PDB code: 5XDW)[85], and *Escherichia coli* (EcFtsZ, PDB code: 6UNX), have been elucidated with significant structural similarity (Supporting Information Fig. S1), revealing conserved domains critical for GTP binding, hydrolysis, and protofilament assembly.

The FtsZ monomer is an intracellular soluble protein with a molecular weight of approximately 40 kDa. FtsZ adopts at least two distinct conformations—relaxed (R) and tense (T)—both essential for its role in cell division[9] but are different in three parts: the GDP-binding site especially the H7 helix, the T7 loop, and the C-terminal subdomain. Notable change between the two states is the conformation of the T7 loop, which is associated with the transition from T to R and *vice versa*[85-87]. In the T state, the T7 loop forms a more defined arrangement by approaching the S9 strand of the C-terminal subdomain and coordinating a metal ion. This stabilizes the opening of the binding cleft, and the formation of filament structure. In contrast, in the R state, the T7 loop adopts a distinct conformation, lacking metal ion coordination and disrupting the terminal helical structure of the H7 helix, eventually allowing the C-terminal subdomain to rotate inward toward the H7 helix and closing the binding cleft. Consistent with these features, the interface areas between neighboring monomers in the filaments were found to be 1,168 $Å^2$ and 798 $Å^2$ in the T and R states, respectively, for SaFtsZ. Such reduction in interface area of the R state causes a gap in one side of the protofilament, which may induce protofilament bending (Fig. 4A[10,82,85,88,89]).

Apart from the T7 loop, the T3 loop also exhibits significant conformational variability across different species (Fig. 4B). In PaFtsZ, the T3 loop is contracted inward, a conformation associated with GDP binding. Conversely, in MtbFtsZ, the T3 loop adopts a more open conformation, enabling it to interact with an adjacent FtsZ monomer within the same protofilament. In *Klebsiella pneumoniae* FtsZ (KpFtsZ), the T3 loop shows distinct conformations depending on the structural state—whether in straight protofilaments (X-ray structure) or in a double-helical tube (cryo-EM structure)—likely influenced by the polymerization packing. These observations highlight that the T3 loop conformation is affected by both nucleotide binding and intermonomer interactions[10].

Recent advances in cryo-EM technology have enabled near *in situ* visualization of FtsZ structures. As shown in Fig. 4C, the cryo-EM single filament of KpFtsZ[89] adopts the T conformation almost identical to the SaFtsZ T state[85], with notable differences at the H1 helix and T7 loop, whereas the straight-filament X-ray model remains locked in the R state[10], exhibiting more pronounced overall divergence. The cryo-EM double-helical tube of KpFtsZ[89], although R-like and convergent with the X-ray protofilament[10] at the S9 strand and H7 helix, reveals significant deviations in the T3 loop and lateral interface geometry. These findings underscore the superior ability of cryo-EM to capture native conformational dynamics and highlight how these assembly-specific features can be exploited to guide the rational design of more potent and selective FtsZ inhibitors. Low-resolution cryo-EM maps of EcFtsZ protofilaments revealed Z-ring reconstitution in liposomes[90,91], while structures of single protofilaments (Fig. 4D) and double-helical tubes (Fig. 4E) of KpFtsZ (PDB codes: 8IBN and 8H1O, respectively) further display its structural diversity[89]. Despite the high sequence conservation, FtsZ from different bacteria still shows notable characteristics related to assembly or interaction with associated proteins, which mainly originate from the C-terminal domain, particularly the less conserved C-terminal tail region[92] or the variable spacer. However, due to the structural disorder in this region, they are not visible in current crystallographic or cryo-EM structures.

7. Binding modes of FtsZ inhibitors

Based on the 215 experimental activity data points collected from 2003 to 2024 (Table 1), we have built a network representing the relationship between FtsZ inhibitors and their targeted bacterial species (Fig. 5A[75]). Currently characterized FtsZ inhibition mainly focuses on four bacterial species: *Escherichia coli* (32 inhibitors), *Bacillus subtilis* (30 inhibitors), *Staphylococcus aureus* (31 inhibitors), and *Mycobacterium tuberculosis* (28 inhibitors). Of note, 15 inhibitors were reported with activities

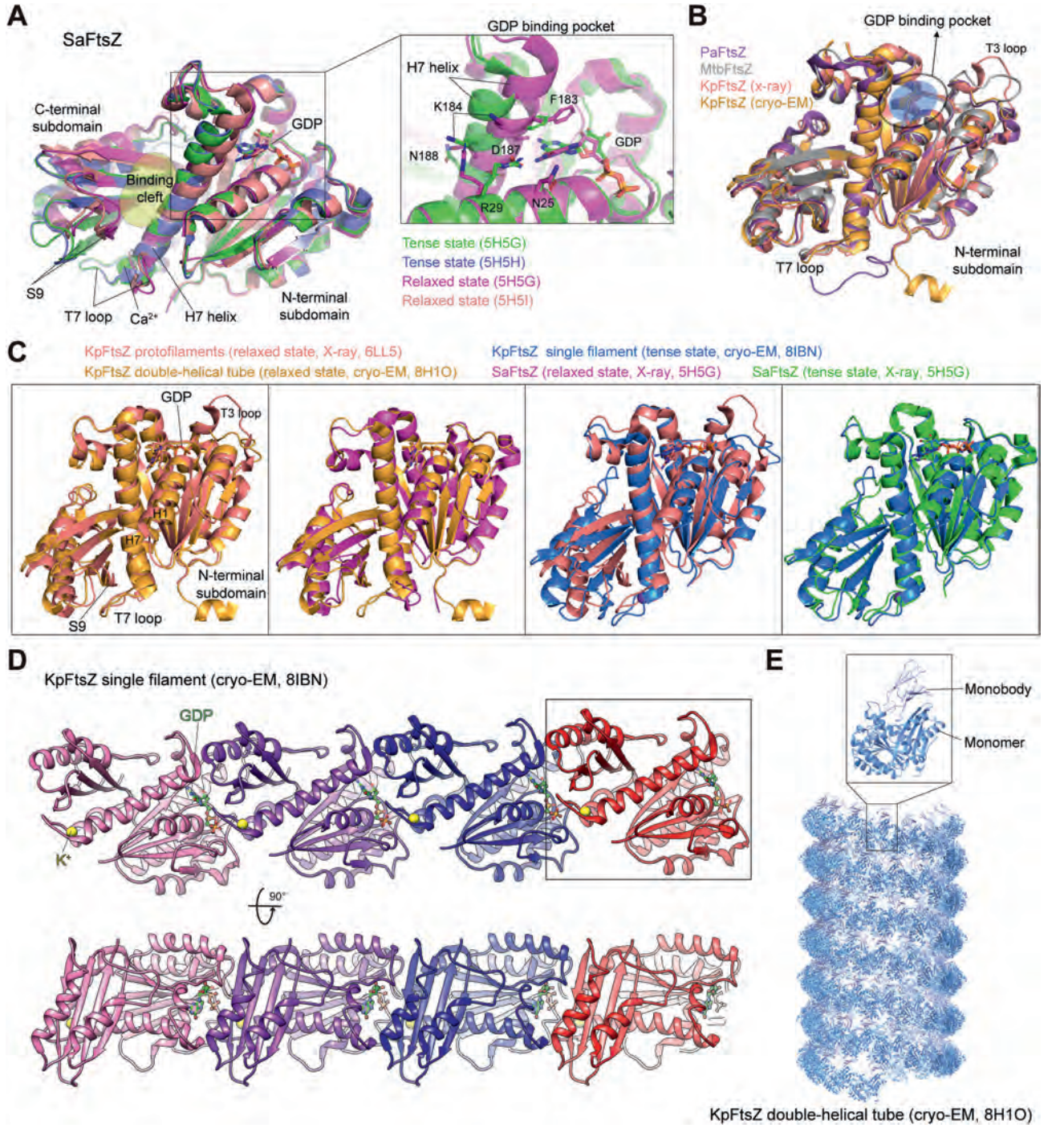

Figure 4 High-resolution structure of the FtsZ monomer, single protofilament and double-helical tube. (A) Crystal structures of *Staphylococcus aureus* FtsZ (SaFtsZ) reveal two distinct conformational states: a relaxed (R) state (PDB codes: 5H5H and 5H5G) and a tense (T) state (PDB codes: 5H5I and 5H5G)[85]. The observation of both conformations within a single crystal (PDB code: 5H5G) underscoring the intrinsic structural equilibrium between these two states. A close-up view highlights the distinct side chain orientations of residues in the T7 helix that surround the GDP binding pocket. (B) Superimposed of crystal structures of *Pseudomonas aeruginosa* FtsZ (PaFtsZ) (PDB code: 2VAW)[82], *Klebsiella pneumoniae* FtsZ in straight protofilaments (KpFtsZ) (PDB code: 6LL5)[10], *Mycobacterium tuberculosis* FtsZ (MtbFtsZ) (PDB code: 4KWE)[88] and cryo-EM structure of KpFtsZ in a double-helical tube (PDB code: 8H1O)[89]. (C) Comparison of KpFtsZ and SaFtsZ structures resolved by X-ray crystallography and cryo-EM. (D) Cryo-EM structure of KpFtsZ protofilament with each monomer shown in a distinct color (PDB code: 8IBN)[89]. The black boxes indicate a single KpFtsZ monomer. (E) Cryo-EM structure of the KpFtsZ double-helical tube. The inset shows a KpFtsZ monomer binding with a Mb (PDB code: 8H1O)[89].

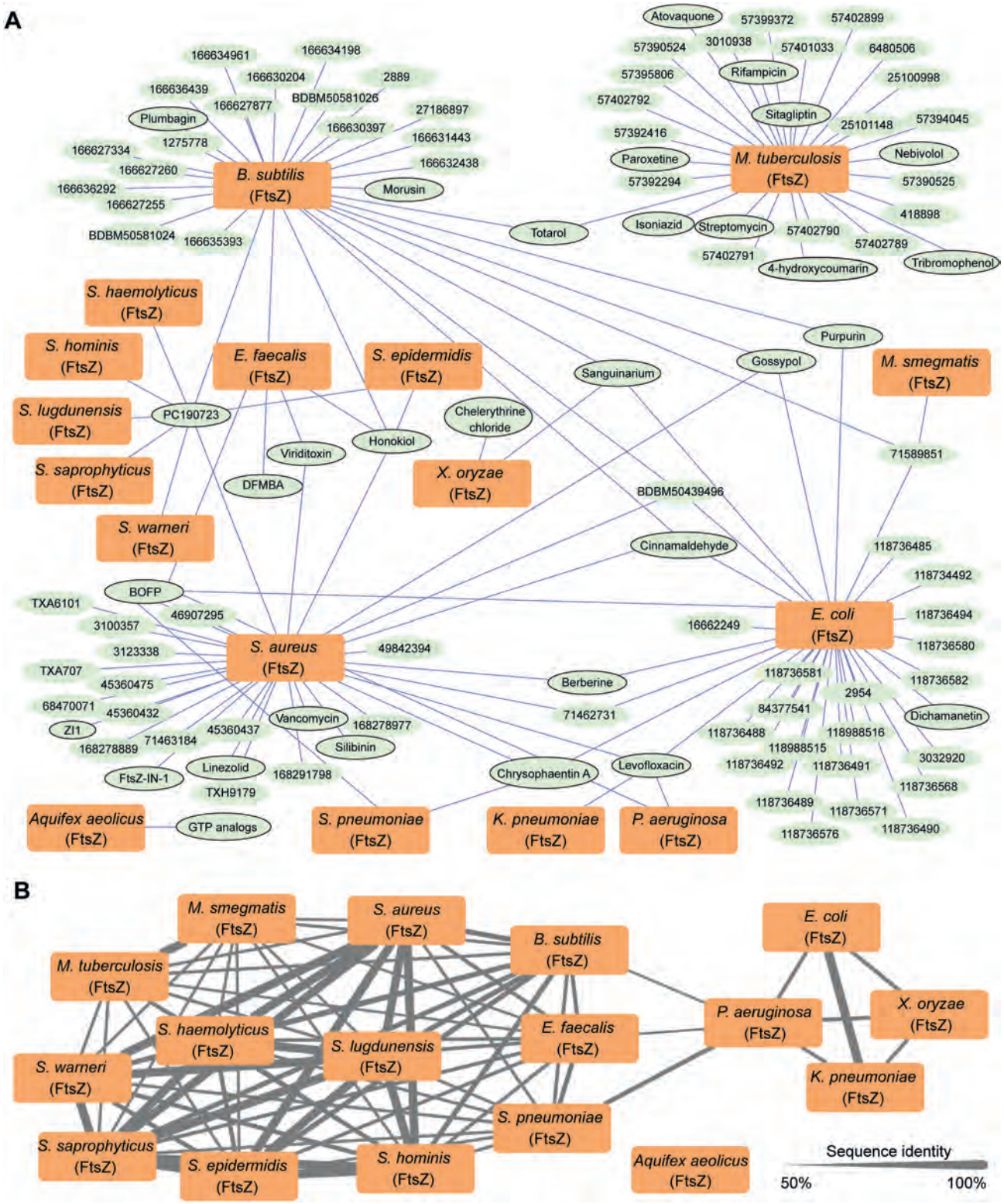

Figure 5 Mapping of FtsZ inhibitors and their targeted bacterial species. (A) Interaction network of FtsZ inhibitors with bacterial FtsZ protein, visualized by Cytoscape v.3.10.2[75]. Green nodes represent FtsZ inhibitors, and orange rectangular nodes denote bacterial species. Edges indicate experimentally validated inhibitory activity agonist bacterial FtsZ. (B) Sequence similarity network of FtsZ across diverse bacterial species. Network visualized using Cytoscape v.3.10.2, with edge thickness reflecting sequence identity[75].

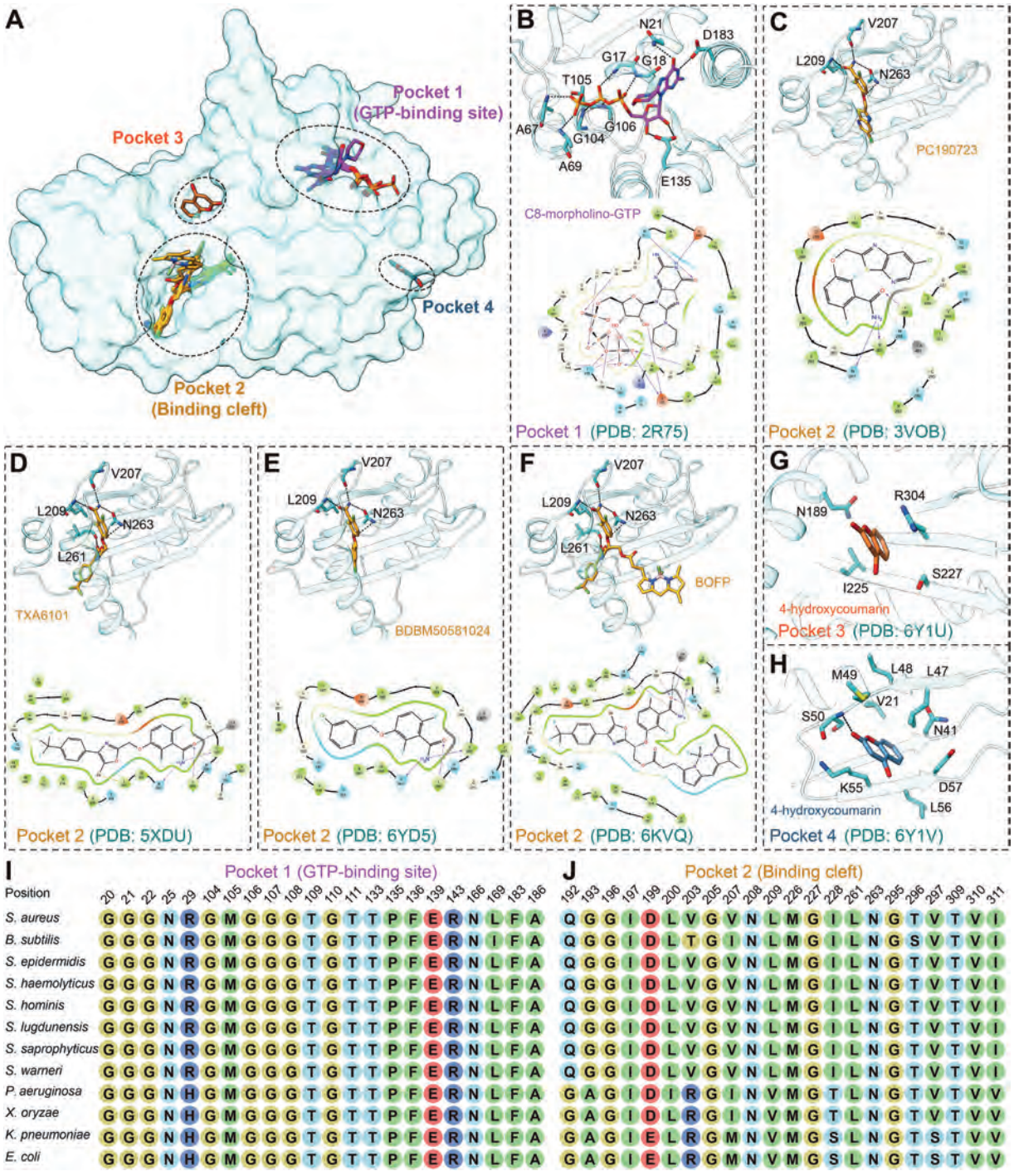

Figure 6 Structural insights into the interaction between FtsZ and inhibitors. (A) Overlay of representative FtsZ structures highlighting four inhibitor-binding pockets[29,32,37,43,60,86]: the GTP-binding site (Pocket 1), a binding cleft adjacent to the T7 loop (Pocket 2), and two allosteric sites (Pockets 3 and 4). (B) Binding mode of C8-morpholino-GTP within Pocket 1 of FtsZ[29], with polar contacts depicted as black dashed lines. (C−F) Binding modes of representative inhibitors within Pocket 2[37,43,60,86]. (G, H) Binding mode of 4-hydroxycoumarin in Pocket 3 (chocolate) and Pocket 4 (steel blue)[32]. (I) Multiple sequence alignments of Pocket 1 (GTP-binding site) residues across representative species. (J) Multiple sequence alignments of Pocket 2 (binding cleft adjacent to the T7 loop) residues across representative species.

against more than one species. For instance, PC190723 is active in eight species, BOFP in five species, followed by chrysophaentins A, levofloxacin and honokiol (four species each), BDBM50439496, cinnamaldehyde, gossypol, PubChem ID 71589851 and sanguinarine (three species each), berberine, PubChem ID 71462731, purpurin, totarol, and viriditoxin (two species each). Sequence-similarity analysis of FtsZ indicates two major phylogenetic classes among these bacteria, suggesting that future inhibitor screens should include representatives from both classes (Fig. 5B).

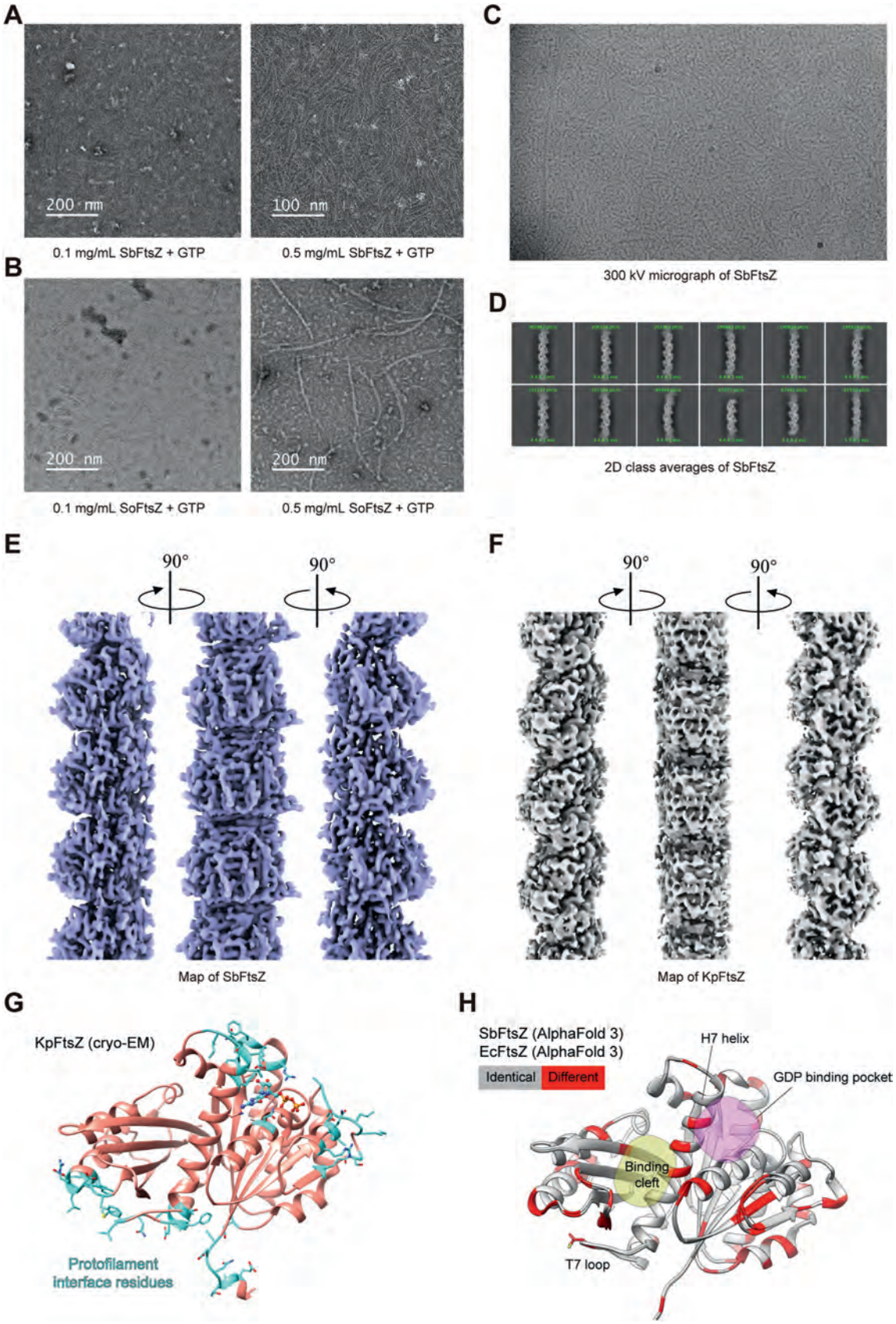

Figure 7 EM analysis of the SbFtsZ single protofilament. (A, B) Various morphologies of SbFtsZ and SoFtsZ filaments. Representative negative-staining micrographs of 0.1 mg/mL SbFtsZ (A) and 0.1 or 0.5 mg/mL SoFtsZ (B) supplemented with 1 mmol/L GTP. (C) Representative cryo-EM micrograph (81,000 × magnification) of SbFtsZ supplemented with 1 mmol/L GTP. (D) Representative 2D class averages of SbFtsZ

Further structural mapping of these reported inhibitors onto FtsZ structures discloses at least four binding pockets (Fig. 6[29,32,37,43,60,86]): the orthosteric GTP-binding site (Pocket 1), a binding cleft adjacent to the T7 loop (Pocket 2), and two cryptic allosteric sites (Pockets 3 and 4). In Pocket 1 (Fig. 6A), C8-morpholino-GTP—a GTP analogue bearing a hydrophobic C8 substituent—inhibits *Aquifex aeolicus* FtsZ with IC_{50} values of 139 μmol/L (polymerization) and 179 μmol/L (GTPase) and a binding affinity of 714 nmol/L (PDB code: 2R75)[29] (Fig. 6B). Pocket 2 accommodates a diverse array of inhibitors including PC190723 (PDB code: 3VOB)[86], TXA6101 (PDB code: 5XDU)[60], BDBM50581024 (PDB code: 6YD5)[37], and BOFP (PDB code: 6KVQ)[43], with distinct binding modes that modulate species selectivity and inhibitory potency (Fig. 6C−F). Notably, 4-hydroxycoumarin binds exclusively to two cryptic pockets in nucleotide-free FtsZ, thereby stabilizing the H7 helix and revealing a conformationally flexible site absent from GTP/GDP co-crystals (PDB codes: 6Y1U and 6Y1V)[32] (Fig. 6G and H). It is conceivable that cryo-EM studies of inhibitor-bound filaments will validate these pockets under native assembly conditions, excluding potential crystal-packing artefacts.

Together, these findings highlight two main challenges. Orthosteric inhibitors face a trade-off between potency and broad-spectrum efficacy, as the GTP-binding site is highly conserved (Fig. 6I). Allosteric pockets offer selectivity but differ markedly across species and assembly states (Fig. 6J). Rational design of next-generation FtsZ inhibitors will therefore require an integrated strategy combining cross-species biochemical profiling with ensemble docking against both X-ray and cryo-EM conformers. This approach should unmask conserved hot-spots and enable optimization of compounds with enhanced potency, specificity, and spectrum.

8. Insights from deepsea SbFtsZ

The remarkable environmental resilience of organisms in extreme conditions, such as high pressures and salinities[93], poses intriguing questions about the adaptability of cellular mechanisms like division. Therefore, FtsZ from deepsea *Shewanella benthic*a (SbFtsZ) may offer valuable insights into the common assembly mechanism and the feasibility of inhibiting it as a therapeutic strategy. Notably, no FtsZ-targeting inhibitors have progressed beyond phase 2 clinical trials, underscoring challenges in disrupting this critical machinery. To investigate molecular determinants of FtsZ functionality under extreme conditions, we determined the cryo-EM structure of SbFtsZ from a deepsea bacterium living in the Mariana Trench's Challenger Deep (Supporting Information Figs. S2 and S3).

Various morphologies of SbFtsZ polymers under negative staining EM in different protein concentrations were observed. SbFtsZ could form thin but clear filaments at both 0.1 and 0.5 mg/mL protein concentrations with the presence of GTP (Fig. 7A[11,89]), consistent with previous studies[94-96]. In contrast, SoFtsZ (the FtsZ in the pressure-sensitive *Shewanella oneidensis* MR-1) originally isolated from Lake Oneida, exhibited different filament formation behavior. At 0.1 mg/mL with GTP, thin filaments were difficult to recognize, whereas at 0.5 mg/mL, bundle filaments were formed, indicating that the protein was likely unstable under the experimental conditions (Fig. 7B).

Based on these findings, we proceeded with cryo-EM structure determination of SbFtsZ, which was prepared at 0.1 mg/mL in the presence of 1 mmol/L GTP, yielding thin and long filaments under 300 kV cryo-EM imaging (Fig. 7C), consistent with the morphology observed under negative staining EM (Fig. 7A). Two-dimensional (2D) class averages showed FtsZ monomers aligning to form protofilaments (Fig. 7D). The final 3D map, reconstructed at 2.94 Å resolution (Fig. S3), represents a single protofilament of SbFtsZ with a helical rise of 44.3 Å and a helical twist of 0.09° (Fig. 7E). However, one view of the map displayed significant stretch, making it challenging to trace the main chain in some regions. A similar situation was observed in the KpFtsZ map (Fig. 7F), where bending of protofilaments in a specific direction prevented optimal particle orientations, thus affecting the final reconstruction quality and structure modelling. This structural conservation implies a robust mechanistic constraint in FtsZ polymerization across diverse taxa, despite extreme environmental adaptation by *Shewanella benthica*.

To gain further insights, we employed AlphaFold 3 to predict its structure[11] and compared it with EcFtsZ. The high accuracy of AlphaFold 3 predictions is demonstrated by the low Cα root mean square deviation (RMSD) (0.4−0.7 Å) between the predicted structure of EcFtsZ and its experimentally determined structure (Supporting Information Fig. S4A). SbFtsZ and EcFtsZ share high sequence homology, with a sequence similarity of 91.0% and a sequence identity of 70.9%. Therefore, AlphaFold 3-predicted SbFtsZ and EcFtsZ structures reveal an alike overall fold, with a Cα RMSD of 0.2 Å (Fig. S4B and S4C). Comparative analysis of protofilament interfaces showed conserved interaction networks: residues surrounding the GDP-binding pocket mediate longitudinal contacts with preceding monomers, while the C-terminal subdomain—particularly the T7 loop—engages the subsequent subunit. Strikingly, only 2 of 30 interfacial residues differ between EcFtsZ (X-ray structure) and SbFtsZ, suggesting evolutionary selection of assembly robustness rather than environment adaptation. This interfacial conservation persists even in KpFtsZ (cryo-EM structure), where directional protofilament curvature arises from lattice packing rather than sequence divergence.

To evaluate the potential impact of sequence differences on FtsZ assembly, we analyzed the interface residues in EcFtsZ (from X-ray) and KpFtsZ (from cryo-EM) (Fig. 7G and H). These residues, particularly those around the GDP-binding pocket, interact with the preceding monomer, while the C-terminal subdomain, especially the T7 loop, interacts with the following monomer. For KpFtsZ, 44 residues involved in assembly (within 5 Å) had only 9 variations in SbFtsZ, whereas for EcFtsZ, 39 residues involved in assembly had 12 variations in SbFtsZ. This suggests that FtsZ assembly does not rely on highly specific conformations or amino acid compositions. In spite of the deepsea environmental pressures, these structural differences do not affect the ability of relevant proteins to participate in bacterial cell division, indicating that FtsZ assembly is relatively adaptable and can function under different conditions.

obtained from 300 kV cryo-EM data collection. (E) Sharpened map of the SbFtsZ single protofilament shown in three views, with an resolution of 3.09 Å. (F) Map of the KpFtsZ single protofilament (EMDB: EMD-35344) presented in three views. (G) Protofilament interface residues in KpFtsZ (PDB code: 8IBN)[89]. (H) Sequence conservation analysis of SbFtsZ and EcFtsZ, mapped onto the AlphaFold 3-predicted structures[11]. Conserved residues are displayed in light gray, while differing residues are highlighted in red.

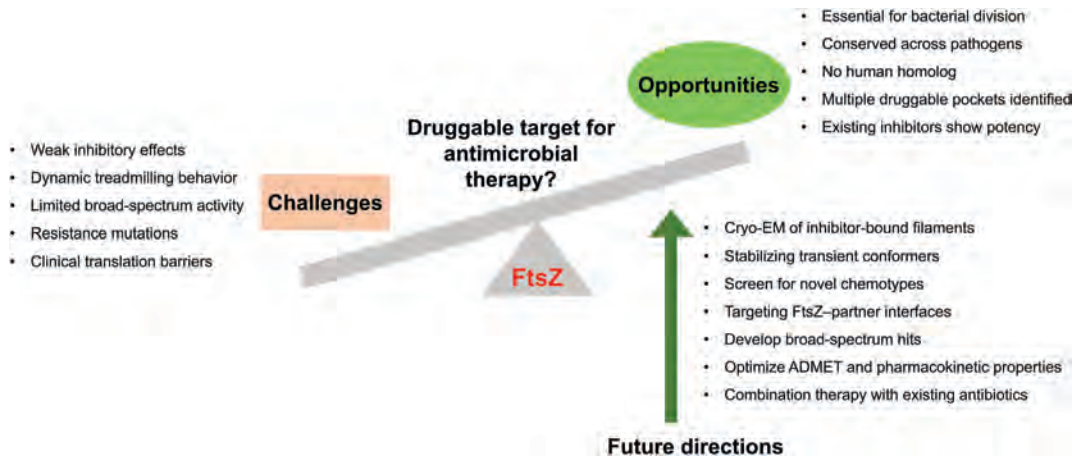

Figure 8 Schematic illustrating the opportunities, challenges, and future strategies for targeting FtsZ in antimicrobial drug development. Using a teeter-totter metaphor to visualize its dual druggability, the elevated right side highlights its essential, conserved role in bacterial cytokinesis (absent in eukaryotes), the presence of multiple ligand-binding pockets and numerous reported inhibitors. The lowered left side depicts key obstacles such as weak inhibitory potency, dynamic treadmilling with tense-relaxed conformational transitions, limited broad-spectrum activity, resistance-conferring mutations, and barriers to translational progress. Beneath the teeter-totter, a horizontal arrow represents future strategies poised to tip the balance toward clinical validation and the development of clinically viable FtsZ inhibitors.

9. Challenges and future directions

The growing prevalence of bacterial resistance underscores an urgent need for new antimicrobial agents with novel mechanisms of action. Traditional antibiotics, which target nucleic acids, protein translation, cell wall synthesis, etc., are becoming less effective due to the rise of multidrug-resistant bacteria. Consequently, alternative targets essential to bacterial survival have become a focal point in drug discovery. FtsZ has thus been implicated as a potential target in this regard. First, FtsZ is the key enzyme involved in bacterial cell division. Second, it is highly conserved across bacterial species, including drug-resistant strains and deadly pathogens such as *Mycobacterium tuberculosis*. Among all bacterial division proteins, FtsZ has the highest level of conservation and sequence similarity, making it less prone to mutations. Third, FtsZ is uniquely present in bacteria, with less than 20% sequence similarity to human tubulin, rendering it suitable to design selective inhibitors that only recognize bacterial FtsZ.

Despite these advantages of FtsZ, currently available FtsZ inhibitors have relatively weak dissociation constant (K_d) values (Table 1). For example, totarol has a K_d of about 11 ± 2.3 μmol/L for *Mycobacterium tuberculosis* FtsZ[50], while certain benzamides such as compound 17 and OTBA (3-{5-[4-oxo-2-thioxo-3-(3-trifluoromethylphenyl)-thiazolidin-5-ylidenemethyl]-furan-2-yl}-benzoic acid) show K_d values ranging from 0.5 to 15 ± 1.5 μmol/L, respectively[73,97]. In comparison, mant-GTP[98] binds to free FtsZ with a K_d of 1.7 ± 0.2 μmol/L[4], which seems physiologically tuned to allow dynamic polymerization and rapid turnover of FtsZ—features essential for bacterial cytokinesis. The dynamic nature of FtsZ polymerization complicates the competitive binding environment for inhibitors. When FtsZ polymerizes into filaments to form the Z-ring, allosteric effects and structural changes may enhance GTP affinity, making it harder for inhibitors to displace GTP effectively. Allosteric FtsZ inhibitors do not directly compete with GTP at the nucleotide-binding site, which reduces cross-reactivity with eukaryotic tubulin but often results in lower binding affinities. These inhibitors are only marginally potent in competitive binding assays because the allosteric pockets are less well-defined. Additionally, bacterial growth conditions and species-specific sequence differences confound the translation of *in vitro* binding affinity into effective *in vivo* inhibition.

To meet such challenges, several strategies could be devised. First, high-resolution crystallography or cryo-EM structures would provide valuable insights into inhibitor binding relative to GTP, helping optimize affinity and specificity. Second, complete understanding of conformational transitions of FtsZ may identify intermediate states[99,100] where allosteric inhibitors can lock FtsZ and suppress its function, similar to kinase inhibitors used in cancer treatments (*e.g.*, asciminib[101] and trametinib[102]). Third, the expansion of chemical libraries, including billion-molecule and marine chemical databases, combined with machine-learning models and high-throughput screening (both virtual and experimental) might uncover new FtsZ inhibitors. Finally, improving the physicochemical properties of existing FtsZ inhibitors, particularly in terms of ADMET (absorption, distribution, metabolism, excretion, and toxicity), remains critical for their clinical application.

FtsZ inhibitors face significant resistance due to its structural plasticity, which enables evolutionary adaptation under selective pressure while preserving core functions like GTP hydrolysis and cytokinesis. For instance, mutations such as G196S (the most common resistance mutation in SaFtsZ)[103,104] and G193D in *Staphylococcus aureus*[105], alongside G196A in *Bacillus subtilis* (which confers resistance to PC190723 but retains sensitivity to 3-MBA)[54,68], highlight key resistance hotspots. Similarly, FtsZ substitutions at residues G196, G193, and N263 are linked to resistance against TXA707 in MRSA[60], with N263K in *Bacillus subtilis* demonstrating complete resistance to both PC190723 and 3-MBA[104]. To address resistance, rational design strategies have yielded inhibitors like TXA6101, which retains activity against MRSA strains harboring G196S or G193D mutant FtsZ[60]. Structural comparisons reveal that the enhanced flexibility of TXA6101 compared to TXA707 allows it to avoid steric clashes with S196 and D193 in SaFtsZ. These structural insights underscore critical determinants for overcoming drug resistance in SaFtsZ and

provide a foundation for designing FtsZ inhibitors with improved antibacterial potency and reduced susceptibility to mutational resistance. Novel chemotypes, such as marine-derived chrysophaentins, competitively inhibit FtsZ and disrupt Z-ring formation in live bacteria, offering a promising chemical space for further investigation[36]. Allosteric inhibitors like PC190723, which target the cleft between nucleotide-binding and GTPase-activating domains of FtsZ, exemplify how binding site selection can mitigate resistance. For example, T5S1607—another predicted allosteric inhibitor—rapidly kills bacteria by inducing FtsZ aggregation, thereby blocking division and causing bacterial death[44]. Combination therapies synergizing FtsZ inhibition with existing antibiotics represent another viable strategy. The 1-methylquinolinium iodide derivative (compound 1)[78] potently inhibits FtsZ polymerization and GTPase activity, demonstrating a broad-spectrum antibacterial activity against drug-resistant strains. Notably, compound 1 enhances β-lactam efficacy in MRSA, while TXA707 shows strong synergy with diverse β-lactams (including cephalosporin, penicillin, and carbapenems)[79]. These findings highlight the potential of structurally optimized FtsZ inhibitors and combinatorial approaches to overcome drug resistance.

However, our cryo-EM studies on SbFtsZ point to a different situation. The extreme conditions of the deepsea, characterized by high-pressure, low-temperature, and high-salinity, provide a tough environment for microorganisms like *Shewanella benthica*. In which, the structural resilience of FtsZ demonstrates its ability to preserve functional integrity. This brings about the challenges of targeting FtsZ therapeutically. Its inherent plasticity allows for rapid reassembly after disruption (*e.g.*, broken filaments can reassemble, and displaced subunits can be replaced), making it a highly adaptable protein. This point of view is consistent with the assembly patterns observed in cryo-EM, where SbFtsZ forms well-aligned protofilaments. Furthermore, inhibiting the core domain of FtsZ does not significantly impede the recruitment of other proteins or the formation of the Z-ring, as these interactions primarily occur through the C-terminal region of FtsZ, which is sequence-diverse and varies in length across species. This suggests that inhibiting the initial assembly or subsequent ring formation is inherently difficult. Nonetheless, the possibility of developing antibiotics that suppress recruitment of other proteins by FtsZ cannot be ruled out. Future studies should be directed toward the elucidation of the interaction between FtsZ and other cell division proteins as well as the expansion of the FtsZ inhibitor pool.

10. Conclusions

FtsZ represents a compelling antibacterial target owing to its indispensable role in driving bacterial cytokinesis through GTP-dependent polymerization into the Z-ring, a mechanism conserved across key pathogens yet distinct from eukaryotic tubulin (Fig. 8). Structural studies of nearly a hundred X-ray and cryo-EM FtsZ models have uncovered an orthosteric GTP-binding site, a binding cleft between the H7 helix and the C terminus, and two allosteric pockets, providing diverse opportunities for inhibitor engagement. Drug screening and medicinal chemistry efforts have yielded compounds such as benzamides, quinolines, and natural products like totarol that bind FtsZ with low micromolar affinities, disrupt filament assembly, and synergize with β-lactams against MRSA and VRE. Nevertheless, progress toward clinical candidates has been hampered by several challenges: generally weak affinities, dynamic transitions between tense and relaxed states, and treadmilling behavior of FtsZ protofilaments that complicates competitive binding and hinders stable inhibition. Additional obstacles include rapid emergence of resistance mutations and species-specific sequence variability that limits broad-spectrum coverage. To date, only one candidate (TXA709) has completed phase 1 clinical trial, with none advancing to phase 2 due to suboptimal ADMET properties and pharmacokinetics. To overcome these challenges, future efforts should focus on: (1) capturing inhibitor-bound filaments by cryo-EM to validate and refine binding modes under native assembly conditions; (2) identifying and stabilizing transient FtsZ conformers akin to allosteric kinase inhibitors to block biological function; (3) harnessing large-scale virtual and experimental screening — augmented by machine-learning models and marine natural product libraries — to discover novel inhibitory chemotypes; and (4) performing cross-species computational and experimental studies to identify broad inhibitors effective against multiple bacterial species, alongside (5) rigorous ADMET and pharmacokinetics optimization. Finally, probing the interfaces between FtsZ and its partner proteins and pursuing rational combination regimens with existing antibiotics will be essential for developing the next generation of FtsZ inhibitors ready for clinical evaluation.

Acknowledgements

We are indebted to Weijia Zhang for valuable discussion, to Linyu Li, Zhaotong Cong, Nan Tian, Qingning Yuan and Canrong Wu for technical assistance. This work is partially supported the research grant from Sanya Municipality, Hainan 2022KJCX77 (to Dehua Yang, China).

Author contributions

Kaini Hang, Wei Han, Xin Li and Qingtong Zhou performed research and analyzed the data; Dehua Yang and Ming-Wei Wang supervised the study; Kainin Hang, Wei Han, Qingtong Zhou and Ming-Wei Wang wrote the manuscript with inputs from all co-authors.

Conflicts of interest

All the authors declare no conflicts of interest.

Appendix A. Supporting information

Supporting information to this article can be found online at https://doi.org/10.1016/j.apsb.2025.06.008.

References

1. Santana-Molina C, Del Saz-Navarro D, Devos DP. Early origin and evolution of the FtsZ/tubulin protein family. *Front Microbiol* 2022; **13**:1100249.
2. McQuillen R, Xiao J. Insights into the structure, function, and dynamics of the bacterial cytokinetic FtsZ-ring. *Annu Rev Biophys* 2020;**49**:309−41.
3. Yang X, Lyu Z, Miguel A, McQuillen R, Huang KC, Xiao J. GTPase activity-coupled treadmilling of the bacterial tubulin FtsZ organizes septal cell wall synthesis. *Science* 2017;**355**:744−7.

4. Fujita J, Maeda Y, Nagao C, Tsuchiya Y, Miyazaki Y, Hirose M, et al. Crystal structure of FtsA from *Staphylococcus aureus*. *FEBS Lett* 2014;**588**:1879−85.
5. Cameron TA, Vega DE, Yu C, Xiao H, Margolin W. ZipA uses a two-pronged FtsZ-binding mechanism necessary for cell division. *mBio* 2021;**12**:e0252921.
6. Du S, Lutkenhaus J. At the heart of bacterial cytokinesis: the Z ring. *Trends Microbiol* 2019;**27**:781−91.
7. Jindal B, Panda D. Understanding FtsZ assembly: cues from the behavior of its N- and C-terminal domains. *Biochemistry* 2013;**52**: 7071−81.
8. Haranahalli K, Tong S, Ojima I. Recent advances in the discovery and development of antibacterial agents targeting the cell-division protein FtsZ. *Bioorg Med Chem* 2016;**24**:6354−69.
9. Schumacher MA, Ohashi T, Corbin L, Erickson HP. High-resolution crystal structures of *Escherichia coli* FtsZ bound to GDP and GTP. *Acta Crystallogr F Struct Biol Commun* 2020;**76**:94−102.
10. Yoshizawa T, Fujita J, Terakado H, Ozawa M, Kuroda N, Tanaka SI, et al. Crystal structures of the cell-division protein FtsZ from *Klebsiella pneumoniae* and *Escherichia coli*. *Acta Crystallogr F Struct Biol Commun* 2020;**76**:86−93.
11. Abramson J, Adler J, Dunger J, Evans R, Green T, Pritzel A, et al. Accurate structure prediction of biomolecular interactions with AlphaFold 3. *Nature* 2024;**630**:493−500.
12. Wang YT, Liu LT, Hou B, Yao CM, Wang XF, Lu B. Recent advances in studies on FtsZ inhibitors. *Biochem Pharmacol* 2024;**230**: 116551.
13. Margolin W. FtsZ and the division of prokaryotic cells and organelles. *Nat Rev Mol Cell Biol* 2005;**6**:862−71.
14. Lutkenhaus J. FtsZ ring in bacterial cytokinesis. *Mol Microbiol* 1993; **9**:403−9.
15. Erickson HP. FtsZ, a tubulin homologue in prokaryote cell division. *Trends Cell Biol* 1997;**7**:362−7.
16. Erickson HP, Anderson DE, Osawa M. FtsZ in bacterial cytokinesis: cytoskeleton and force generator all in one. *Microbiol Mol Biol Rev* 2010;**74**:504−28.
17. Haeusser DP, Margolin W. Splitsville: structural and functional insights into the dynamic bacterial Z ring. *Nat Rev Microbiol* 2016;**14**: 305−19.
18. Adams DW, Errington J. Bacterial cell division: assembly, maintenance and disassembly of the Z ring. *Nat Rev Microbiol* 2009;**7**: 642−53.
19. Ortiz C, Natale P, Cueto L, Vicente M. The keepers of the ring: regulators of FtsZ assembly. *FEMS Microbiol Rev* 2016;**40**:57−67.
20. Levin PA, Kurtser IG, Grossman AD. Identification and characterization of a negative regulator of FtsZ ring formation in *Bacillus subtilis*. *Proc Natl Acad Sci U S A* 1999;**96**:9642−7.
21. Camberg JL, Hoskins JR, Wickner S. ClpXP protease degrades the cytoskeletal protein, FtsZ, and modulates FtsZ polymer dynamics. *Proc Natl Acad Sci U S A* 2009;**106**:10614−9.
22. Hurley KA, Santos TM, Nepomuceno GM, Huynh V, Shaw JT, Weibel DB. Targeting the bacterial division protein FtsZ. *J Med Chem* 2016;**59**:6975−98.
23. LaBreck CJ, Conti J, Viola MG, Camberg JL. MinC N- and C-domain interactions modulate FtsZ assembly, division site selection, and MinD-dependent oscillation in *Escherichia coli*. *J Bacteriol* 2019;**201**:e00374-18.
24. Luo A, Qian C, Zhang Z, Xia J, Jin H, Si X, et al. Discovery of novel FtsZ inhibitors with antimicrobial activity by virtual screening and *in vitro* biological evaluation. *Chem Biodivers* 2025: e202403042.
25. Margalit DN, Romberg L, Mets RB, Hebert AM, Mitchison TJ, Kirschner MW, et al. Targeting cell division: small-molecule inhibitors of FtsZ GTPase perturb cytokinetic ring assembly and induce bacterial lethality. *Proc Natl Acad Sci U S A* 2004;**101**:11821−6.
26. Mukherjee A, Lutkenhaus J. Analysis of FtsZ assembly by light scattering and determination of the role of divalent metal cations. *J Bacteriol* 1999;**181**:823−32.
27. Domadia P, Swarup S, Bhunia A, Sivaraman J, Dasgupta D. Inhibition of bacterial cell division protein FtsZ by cinnamaldehyde. *Biochem Pharmacol* 2007;**74**:831−40.
28. Stokes NR, Sievers J, Barker S, Bennett JM, Brown DR, Collins I, et al. Novel inhibitors of bacterial cytokinesis identified by a cell-based antibiotic screening assay. *J Biol Chem* 2005;**280**:39709−15.
29. Läppchen T, Pinas VA, Hartog AF, Koomen GJ, Schaffner-Barbero C, Andreu JM, et al. Probing FtsZ and tubulin with C8-substituted GTP analogs reveals differences in their nucleotide binding sites. *Chem Biol* 2008;**15**:189−99.
30. Zhang H, Chen Y, Zhang Y, Qiao L, Chi X, Han Y, et al. Identification of anti-Mycobacterium tuberculosis agents targeting the interaction of bacterial division proteins FtsZ and SepFe. *Acta Pharm Sin B* 2023;**13**:2056−70.
31. Bhondwe P, Sengar N, Bodiwala HS, Singh IP, Panda D. An adamantyl-caffeoyl-anilide exhibits broad-spectrum antibacterial activity by inhibiting FtsZ assembly and Z-ring formation. *Int J Biol Macromol* 2024;**259**:129255.
32. Alnami A, Norton RS, Pena HP, Haider S, Kozielski F. Conformational flexibility of a highly conserved helix controls cryptic pocket formation in FtsZ. *J Mol Biol* 2021;**433**:167061.
33. Tovar-Nieto AM, Flores-Padilla LE, Rivas-Santiago B, Trujillo-Paez JV, Lara-Ramirez EE, Jacobo-Delgado YM, et al. The repurposing of FDA-approved drugs as FtsZ inhibitors against *Mycobacterium tuberculosis*: an *in silico* and *in vitro* study. *Microorganisms* 2024;**12**:1505.
34. Mathew B, Srivastava S, Ross LJ, Suling WJ, White EL, Woolhiser LK, et al. Novel pyridopyrazine and pyrimidothiazine derivatives as FtsZ inhibitors. *Bioorg Med Chem* 2011;**19**:7120−8.
35. Kumar K, Awasthi D, Lee SY, Zanardi I, Ruzsicska B, Knudson S, et al. Novel trisubstituted benzimidazoles, targeting Mtb FtsZ, as a new class of antitubercular agents. *J Med Chem* 2011;**54**:374−81.
36. Keffer JL, Huecas S, Hammill JT, Wipf P, Andreu JM, Bewley CA. Chrysophaentins are competitive inhibitors of FtsZ and inhibit Z-ring formation in live bacteria. *Bioorg Med Chem* 2013;**21**:5673−8.
37. Huecas S, Araujo-Bazan L, Ruiz FM, Ruiz-Avila LB, Martinez RF, Escobar-Pena A, et al. Targeting the FtsZ allosteric binding site with a novel fluorescence polarization screen, cytological and structural approaches for antibacterial discovery. *J Med Chem* 2021;**64**: 5730−45.
38. Kaur S, Modi NH, Panda D, Roy N. Probing the binding site of curcumin in *Escherichia coli* and *Bacillus subtilis* FtsZ—a structural insight to unveil antibacterial activity of curcumin. *Eur J Med Chem* 2010;**45**:4209−14.
39. Li X, Ma S. Advances in the discovery of novel antimicrobials targeting the assembly of bacterial cell division protein FtsZ. *Eur J Med Chem* 2015;**95**:1−15.
40. Du RL, Chow HY, Chen YW, Chan PH, Daniel RA, Wong KY. Gossypol acetate: a natural polyphenol derivative with antimicrobial activities against the essential cell division protein FtsZ. *Front Microbiol* 2022;**13**:1080308.
41. Buroni S, Makarov V, Scoffone VC, Trespidi G, Riccardi G, Chiarelli LR. The cell division protein FtsZ as a cellular target to hit cystic fibrosis pathogens. *Eur J Med Chem* 2020;**190**:112132.
42. Sun N, Zhi Z, Xiao T, Deng X, He T, Dong W, et al. The study of honokiol as a natural product-based antimicrobial agent and its potential interaction with FtsZ protein. *Front Microbiol* 2024;**15**: 1361508.
43. Ferrer-Gonzalez E, Fujita J, Yoshizawa T, Nelson JM, Pilch AJ, Hillman E, et al. Structure-guided design of a fluorescent probe for the visualization of FtsZ in clinically important Gram-positive and Gram-negative bacterial pathogens. *Sci Rep* 2019;**9**:20092.
44. Xie Z, Ruan W, Guo J, Li Y, Zhou S, Zhao J, et al. T5S1607 identified as a antibacterial FtsZ inhibitor:virtual screening combined with bioactivity evaluation for the drug discovery. *Comput Biol Chem* 2024;**108**:108006.
45. Plaza A, Keffer JL, Bifulco G, Lloyd JR, Bewley CA. Chrysophaentins A-H, antibacterial bisdiarylbutene macrocycles that

inhibit the bacterial cell division protein FtsZ. *J Am Chem Soc* 2010; **132**:9069−77.
46. Haydon DJ, Stokes NR, Ure R, Galbraith G, Bennett JM, Brown DR, et al. An inhibitor of FtsZ with potent and selective anti-staphylococcal activity. *Science* 2008;**321**:1673−5.
47. Mahanty S, Rathinasamy K. The natural anthraquinone dye purpurin exerts antibacterial activity by perturbing the FtsZ assembly. *Bioorg Med Chem* 2021;**50**:116463.
48. Song D, Zhang N, Zhang P, Zhang N, Chen W, Zhang L, et al. Design, synthesis and evaluation of novel 9-arylalkyl-10-methylacridinium derivatives as highly potent FtsZ-targeting antibacterial agents. *Eur J Med Chem* 2021;**221**:113480.
49. Kim MB, O'Brien TE, Moore JT, Anderson DE, Foss MH, Weibel DL, et al. The synthesis and antimicrobial activity of heterocyclic derivatives of totarol. *ACS Med Chem Lett* 2012;**3**: 818−22.
50. Jaiswal R, Beuria TK, Mohan R, Mahajan SK, Panda D. Totarol inhibits bacterial cytokinesis by perturbing the assembly dynamics of FtsZ. *Biochemistry* 2007;**46**:4211−20.
51. Kelley C, Zhang Y, Parhi A, Kaul M, Pilch DS, LaVoie EJ. 3-Phenyl substituted 6,7-dimethoxyisoquinoline derivatives as FtsZ-targeting antibacterial agents. *Bioorg Med Chem* 2012;**20**:7012−29.
52. Wang J, Galgoci A, Kodali S, Herath KB, Jayasuriya H, Dorso K, et al. Discovery of a small molecule that inhibits cell division by blocking FtsZ, a novel therapeutic target of antibiotics. *J Biol Chem* 2003;**278**:44424−8.
53. Du RL, Sun N, Fung YH, Zheng YY, Chen YW, Chan PH, et al. Discovery of FtsZ inhibitors by virtual screening as antibacterial agents and study of the inhibition mechanism. *RSC Med Chem* 2022; **13**:79−89.
54. Kaul M, Parhi AK, Zhang Y, LaVoie EJ, Tuske S, Arnold E, et al. A bactericidal guanidinomethyl biaryl that alters the dynamics of bacterial FtsZ polymerization. *J Med Chem* 2012;**55**:10160−76.
55. Zhong DX, She MT, Guo XC, Zheng BX, Huang XH, Zhang YH, et al. Design and synthesis of quinolinium-based derivatives targeting FtsZ for antibacterial evaluation and mechanistic study. *Eur J Med Chem* 2022;**236**:114360.
56. Li X, Sheng J, Huang G, Ma R, Yin F, Song D, et al. Design, synthesis and antibacterial activity of cinnamaldehyde derivatives as inhibitors of the bacterial cell division protein FtsZ. *Eur J Med Chem* 2015;**97**:32−41.
57. Bryan E, Ferrer-Gonzalez E, Sagong HY, Fujita J, Mark L, Kaul M, et al. Structural and antibacterial characterization of a new benzamide FtsZ inhibitor with superior bactericidal activity and *in vivo* efficacy against multidrug-resistant *Staphylococcus aureus*. *ACS Chem Biol* 2023;**18**:629−42.
58. Nepomuceno GM, Chan KM, Huynh V, Martin KS, Moore JT, O'Brien TE, et al. Synthesis and evaluation of quinazolines as inhibitors of the bacterial cell division protein FtsZ. *ACS Med Chem Lett* 2015;**6**:308−12.
59. Basak P, Dastidar DG, Ghosh D, Chakraborty T, Sau S, Chakrabarti G. *Staphylococcus aureus* major cell division protein FtsZ assembly is inhibited by silibinin, a natural flavonolignan that also blocked bacterial growth and biofilm formation. *Int J Biol Macromol* 2024;**279**:135252.
60. Fujita J, Maeda Y, Mizohata E, Inoue T, Kaul M, Parhi AK, et al. Structural flexibility of an inhibitor overcomes drug resistance mutations in *Staphylococcus aureus* FtsZ. *ACS Chem Biol* 2017;**12**: 1947−55.
61. Stokes NR, Baker N, Bennett JM, Chauhan PK, Collins I, Davies DT, et al. Design, synthesis and structure-activity relationships of substituted oxazole-benzamide antibacterial inhibitors of FtsZ. *Bioorg Med Chem Lett* 2014;**24**:353−9.
62. Meng J, Li M, Zheng Z, Sun Z, Yang S, Ouyang G, et al. Application of natural-products repurposing strategy to discover novel FtsZ inhibitors: bactericidal evaluation and the structure-activity relationship of sanguinarine and its analogs. *Pestic Biochem Physiol* 2024; **203**:106016.
63. Domadia PN, Bhunia A, Sivaraman J, Swarup S, Dasgupta D. Berberine targets assembly of *Escherichia coli* cell division protein FtsZ. *Biochemistry* 2008;**47**:3225−34.
64. Sun N, Chan FY, Lu YJ, Neves MA, Lui HK, Wang Y, et al. Rational design of berberine-based FtsZ inhibitors with broad-spectrum antibacterial activity. *PLoS One* 2014;**9**:e97514.
65. Rai D, Singh JK, Roy N, Panda D. Curcumin inhibits FtsZ assembly: an attractive mechanism for its antibacterial activity. *Biochem J* 2008;**410**:147−55.
66. Shi C, Che M, Zhang X, Liu Z, Meng R, Bu X, et al. Antibacterial activity and mode of action of totarol against *Staphylococcus aureus* in carrot juice. *J Food Sci Technol* 2018;**55**:924−34.
67. Ohashi Y, Chijiiwa Y, Suzuki K, Takahashi K, Nanamiya H, Sato T, et al. The lethal effect of a benzamide derivative, 3-methoxybenzamide, can be suppressed by mutations within a cell division gene, ftsZ, in *Bacillus subtilis*. *J Bacteriol* 1999;**181**:1348−51.
68. Kaul M, Mark L, Zhang Y, Parhi AK, Lyu YL, Pawlak J, et al. TXA709, an FtsZ-targeting benzamide prodrug with improved pharmacokinetics and enhanced *in vivo* efficacy against methicillin-resistant *Staphylococcus aureus*. *Antimicrob Agents Chemother* 2015;**59**:4845−55.
69. Foley M, Tilley L. Quinoline antimalarials: mechanisms of action and resistance. *Int J Parasitol* 1997;**27**:231−40.
70. Sun N, Du RL, Zheng YY, Huang BH, Guo Q, Zhang RF, et al. Antibacterial activity of *N*-methylbenzofuro[3,2-*b*]quinoline and *N*-methylbenzoindolo[3,2-*b*]-quinoline derivatives and study of their mode of action. *Eur J Med Chem* 2017;**135**:1−11.
71. Sun N, Lu YJ, Chan FY, Du RL, Zheng YY, Zhang K, et al. A thiazole orange derivative targeting the bacterial protein FtsZ shows potent antibacterial activity. *Front Microbiol* 2017;**8**:855.
72. Ruiz-Avila LB, Huecas S, Artola M, Vergoñós A, Ramírez-Aportela E, Cercenado E, et al. Synthetic inhibitors of bacterial cell division targeting the GTP-binding site of FtsZ. *ACS Chem Biol* 2013;**8**:2072−83.
73. Artola M, Ruiz-Avila LB, Vergoñós A, Huecas S, Araujo-Bazán L, Martín-Fontecha M, et al. Effective GTP-replacing FtsZ inhibitors and antibacterial mechanism of action. *ACS Chem Biol* 2015;**10**: 834−43.
74. Maggiora G, Vogt M, Stumpfe D, Bajorath J. Molecular similarity in medicinal chemistry. *J Med Chem* 2014;**57**:3186−204.
75. Shannon P, Markiel A, Ozier O, Baliga NS, Wang JT, Ramage D, et al. Cytoscape: a software environment for integrated models of biomolecular interaction networks. *Genome Res* 2003;**13**:2498−504.
76. Andreu JM, Schaffner-Barbero C, Huecas S, Alonso D, Lopez-Rodriguez ML, Ruiz-Avila LB, et al. The antibacterial cell division inhibitor PC190723 is an FtsZ polymer-stabilizing agent that induces filament assembly and condensation. *J Biol Chem* 2010;**285**: 14239−46.
77. Sharma AK, Poddar SM, Chakraborty J, Nayak BS, Kalathil S, Mitra N, et al. A mechanism of salt bridge-mediated resistance to FtsZ inhibitor PC190723 revealed by a cell-based screen. *Mol Biol Cell* 2023;**34**:ar16.
78. Ferrer-Gonzalez E, Huh H, Al-Tameemi HM, Boyd JM, Lee SH, Pilch DS. Impact of FtsZ Inhibition on the localization of the penicillin binding proteins in methicillin-resistant *Staphylococcus aureus*. *J Bacteriol* 2021;**203**:e0020421.
79. Ferrer-Gonzalez E, Kaul M, Parhi AK, LaVoie EJ, Pilch DS. β-Lactam antibiotics with a high affinity for PBP2 act synergistically with the FtsZ-targeting agent TXA707 against methicillin-resistant *Staphylococcus aureus*. *Antimicrob Agents Chemother* 2017;**61**:e00863-17.
80. Löwe J, Amos LA. Crystal structure of the bacterial cell-division protein FtsZ. *Nature* 1998;**391**:203−6.
81. Leung AK, Lucile White E, Ross LJ, Reynolds RC, DeVito JA, Borhani DW. Structure of *Mycobacterium tuberculosis* FtsZ reveals unexpected, G protein-like conformational switches. *J Mol Biol* 2004;**342**:953−70.
82. Oliva MA, Trambaiolo D, Löwe J. Structural insights into the conformational variability of FtsZ. *J Mol Biol* 2007;**373**:1229−42.

83. Respicio L, Nair PA, Huang Q, Anil B, Tracz S, Truglio JJ, et al. Characterizing septum inhibition in *Mycobacterium tuberculosis* for novel drug discovery. *Tuberculosis* 2008;**88**:420−9.
84. Raymond A, Lovell S, Lorimer D, Walchli J, Mixon M, Wallace E, et al. Combined protein construct and synthetic gene engineering for heterologous protein expression and crystallization using Gene Composer. *BMC Biotechnol* 2009;**9**:37.
85. Fujita J, Harada R, Maeda Y, Saito Y, Mizohata E, Inoue T, et al. Identification of the key interactions in structural transition pathway of FtsZ from *Staphylococcus aureus*. *J Struct Biol* 2017; **198**:65−73.
86. Matsui T, Yamane J, Mogi N, Yamaguchi H, Takemoto H, Yao M, et al. Structural reorganization of the bacterial cell-division protein FtsZ from *Staphylococcus aureus*. *Acta Crystallogr D Biol Crystallogr* 2012;**68**:1175−88.
87. Campbell C, Fingleton C, Zeden MS, Bueno E, Gallagher LA, Shinde D, et al. Accumulation of succinyl coenzyme A perturbs the methicillin-resistant *Staphylococcus aureus* (MRSA) succinylome and is associated with increased susceptibility to β-lactam antibiotics. *mBio* 2021;**12**:e0053021.
88. Li Y, Hsin J, Zhao L, Cheng Y, Shang W, Huang KC, et al. FtsZ protofilaments use a hinge-opening mechanism for constrictive force generation. *Science* 2013;**341**:392−5.
89. Fujita J, Amesaka H, Yoshizawa T, Hibino K, Kamimura N, Kuroda N, et al. Structures of a FtsZ single protofilament and a double-helical tube in complex with a monobody. *Nat Commun* 2023; **14**:4073.
90. Szwedziak P, Wang Q, Bharat TA, Tsim M, Löwe J. Architecture of the ring formed by the tubulin homologue FtsZ in bacterial cell division. *eLife* 2014;**3**:e04601.
91. Wagstaff JM, Tsim M, Oliva MA, García-Sanchez A, Kureisaite-Ciziene D, Andreu JM, et al. A Polymerization-associated structural switch in FtsZ that enables treadmilling of model filaments. *mBio* 2017;**8**:e00254-17.
92. Battaje RR, Piyush R, Pratap V, Panda D. Models *versus* pathogens: how conserved is the FtsZ in bacteria? *Biosci Rep* 2023;**43**: BSR20221664.
93. Medvedev KE, Kolchanov NA, Afonnikov DA. High temperature and pressure influence the interdomain orientation of Nip7 proteins from *P. abyssi* and *P. furiosus*: MD simulations. *J Biomol Struct Dyn* 2018;**36**:68−82.
94. Huecas S, Llorca O, Boskovic J, Martín-Benito J, Valpuesta JM, Andreu JM. Energetics and geometry of FtsZ polymers: nucleated self-assembly of single protofilaments. *Biophys J* 2008;**94**: 1796−806.
95. Romberg L, Simon M, Erickson HP. Polymerization of Ftsz, a bacterial homolog of tubulin. is assembly cooperative? *J Biol Chem* 2001;**276**:11743−53.
96. Concha-Marambio L, Maldonado P, Lagos R, Monasterio O, Montecinos-Franjola F. Thermal adaptation of mesophilic and thermophilic FtsZ assembly by modulation of the critical concentration. *PLoS One* 2017;**12**:e0185707.
97. Kifayat S, Yele V, Ashames A, Sigalapalli DK, Bhandare RR, Shaik AB, et al. Filamentous temperature sensitive mutant Z: a putative target to combat antibacterial resistance. *RSC Adv* 2023;**13**: 11368−84.
98. Bisson-Filho AW, Discola KF, Castellen P, Blasios V, Martins A, Sforça ML, et al. FtsZ filament capping by MciZ, a developmental regulator of bacterial division. *Proc Natl Acad Sci U S A* 2015;**112**: E2130−8.
99. Knapp BD, Shi H, Huang KC. Complex state transitions of the bacterial cell division protein FtsZ. *Mol Biol Cell* 2024;**35**: ar130.
100. Takasawa T, Matsui T, Watanabe G, Kodera Y. Molecular dynamics simulations reveal differences in the conformational stability of FtsZs derived from *Staphylococcus aureus* and *Bacillus subtilis*. *Sci Rep* 2024;**14**:16043.
101. Wylie AA, Schoepfer J, Jahnke W, Cowan-Jacob SW, Loo A, Furet P, et al. The allosteric inhibitor ABL001 enables dual targeting of BCR-ABL1. *Nature* 2017;**543**:733−7.
102. Khan ZM, Real AM, Marsiglia WM, Chow A, Duffy ME, Yerabolu JR, et al. Structural basis for the action of the drug trametinib at KSR-bound MEK. *Nature* 2020;**588**:509−14.
103. Tan CM, Therien AG, Lu J, Lee SH, Caron A, Gill CJ, et al. Restoring methicillin-resistant *Staphylococcus aureus* susceptibility to beta-lactam antibiotics. *Sci Transl Med* 2012;**4**:126ra35.
104. Adams DW, Wu LJ, Errington J. A benzamide-dependent ftsZ mutant reveals residues crucial for Z-ring assembly. *Mol Microbiol* 2016;**99**: 1028−42.
105. Pereira AR, Hsin J, Król E, Tavares AC, Flores P, Hoiczyk E, et al. FtsZ-dependent elongation of a coccoid bacterium. *mBio* 2016;**7**: e00908−16.